学位論文

DOK7 gene therapy in a mouse model of amyotrophic lateral sclerosis

（筋萎縮性側索硬化症モデルマウスに対する
DOK7 遺伝子治療の効果とその作用機序）

平成 28 年 12 月博士（理学）申請

東京大学大学院理学系研究科
生物科学専攻
三好 貞徳

Abstract

Amyotrophic lateral sclerosis (ALS) is a progressive, multifactorial degenerative disease of motor neurons with severe muscle atrophy. The glutamate release inhibitor riluzole and the free radical scavenger edaravone are the only medications approved in Japan for ALS, but their therapeutic effects are limited, testifying to the strong need for new treatment strategies. In ALS, degeneration of motor nerve terminals at the neuromuscular junction (NMJ), the cholinergic synapse between a motor neuron and skeletal muscle, precedes proximal motor neuron degeneration, termed “dying-back” pathology, implicating the NMJ as a therapeutic target. However, a promising NMJ-targeted therapy for ALS has not been developed to date.

The muscle protein Dok-7 is an essential activator of the muscle-specific kinase MuSK, which governs NMJ formation and maintenance. Dok-7 directly interacts with the cytoplasmic portion of MuSK and activates the receptor kinase. Indeed, recessive mutations in the human *DOK7* gene cause a congenital myasthenic syndrome (*DOK7* myasthenia) with defective NMJ structure. On the other hand, forced expression of Dok-7 in muscle activates MuSK and enlarges NMJs. Our laboratory previously generated AAV-D7, an adeno-associated virus vector carrying the human *DOK7* gene tagged with the enhanced green fluorescent protein under the control of the cytomegalovirus promoter, and demonstrated that the therapeutic administration of AAV-D7 (*DOK7* gene therapy)

enlarges NMJs and enhances motor activity and life span in a mouse model of *DOK7* myasthenia. In addition, *DOK7* gene therapy improves motor function and survival in a mouse model of autosomal dominant Emery–Dreifuss muscular dystrophy, a disease with defective NMJs due to mutations in the lamin A/C gene. These observations demonstrate that *DOK7* gene therapy may be effective in these myopathies with NMJ defects. I suspected that this therapy might also benefit ALS because the forced expression of Dok-7 in muscle enlarges NMJs not only at postsynaptic acetylcholine receptor (AChR) clusters, but also presynaptic motor nerve terminals, which might counteract size reductions and denervation of the terminal. Motor nerve terminal defects appear to play an important role in the pathogenesis of ALS in both patients and animal models; accordingly, I examined whether *DOK7* gene therapy benefits a mouse model of ALS.

In ~20% of familial cases of ALS, patients harbor a gain-of-function mutation in the gene encoding Cu/Zn superoxide dismutase 1 (SOD1). Mice expressing human SOD1 (hSOD1) with the ALS-linked G93A mutation (hereafter, ALS mice) are widely used as an animal model because they manifest progressive muscle paralysis similar to that observed in clinical cases, along with the histopathological hallmarks observed in familial and sporadic ALS, including NMJ defects.

First, I examined the effect of forced expression of Dok-7 on the histopathology of NMJs, skeletal muscles, and motor neurons in ALS mice. I intravenously administered

AAV-D7 to male ALS mice at an early symptomatic stage (postnatal day 90, P90) and performed histological analyses 30 days later. Based on confocal microscopic analyses of NMJs, I found that AAV-D7 treatment enlarged motor nerve terminals at NMJs, in addition to postsynaptic AChR clusters, indicating positive effects on motor neurons. Indeed, denervation at NMJs was suppressed, demonstrating that *DOK7* gene therapy had a protective effect against nerve terminal degeneration in ALS mice. Moreover, *DOK7* gene therapy further suppressed muscle atrophy in ALS mice, supporting the notion that NMJ defects are a cause of muscle atrophy in ALS. I also examined the effect of AAV-D7 treatment on progressive motor neuron death, another hallmark of ALS, and found no significant differences between treated and untreated mice. Together, these results indicate that *DOK7* gene therapy suppressed NMJ defects and muscle atrophy in ALS mice and had no obvious effects on proximal motor neuron degeneration at 30 days post-infection.

Second, I examined the effects of *DOK7* gene therapy, AAV-D7 treatment initiated after disease onset, on the survival and motor activity of ALS mice. Individuals with ALS are usually diagnosed after the onset of symptoms. Therefore, to strictly evaluate the potential of AAV-D7 as a therapy, I defined disease onset in each male ALS mouse individually by monitoring its grip strength, and at this individually defined disease onset, administered AAV-D7 for a survival analysis according to the guidelines for pre-clinical ALS studies.

Note that this guideline was recently established to improve translation to humans, mainly because many, if not all, beneficial life span effects obtained in clinical trials using ALS mice have failed to translate to humans. Remarkably, recent studies using experimental settings that fit this guideline reported that even riluzole and other drugs that had been reported to enhance survival of ALS model mice failed to prove their efficacy in ALS mice. I show here, in a study fully adhering to the guideline, that *DOK7* gene therapy prolonged not only mouse lifespan, but also the duration of survival after onset. Furthermore, using the automated home cage behavioral system, I demonstrate that *DOK7* gene therapy enhanced spontaneous motor activity.

Together, my findings demonstrate the importance of NMJ pathology in ALS and provide evidence that *DOK7* gene therapy or an equivalent method that enlarges NMJs has that potential to treat not only myopathies, but also motor neuron diseases that manifest NMJ defects.

Contents

Abbreviations

AAV: adeno-associated virus

ACh: acetylcholine

AChR: ACh receptor

ADAR2: adenosine deaminase acting on RNA

AD-EDMD: autosomal dominant Emery-Dreifuss muscular dystrophy

ALS: amyotrophic lateral sclerosis

AMPA: α-amino-3-hydroxy-5-methyl-4-isoxazolepropionic acid

ANOVA: analysis of variance

BAX: Bcl-2-associated X protein

BSA: bovine serum albumin

CMV: cytomegalovirus

CSA: cross-sectional area

Ct: cycle threshold

DOK7 or Dok-7: downstream of tyrosine kinases 7

DNA: deoxyribonucleic acid

EGFP: enhanced green fluorescent protein

FGFBP1: fibroblast growth factor-binding protein 1

GDNF: glial cell-derived neurotrophic factor

HSA: human skeletal α-actin

IP: immunoprecipitation

LPL: lipoprotein lipase

Lrp4: low-density lipoprotein receptor-related protein 4

MuSK: muscle specific tyrosine kinase

NMDA: *N*-methyl-D-aspartate

NMJ: neuromuscular junction

PBS: phosphate buffered saline

PCR: polymerase chain reaction

PFA: paraformaldehyde

pY: phosphotyrosine

RNA: ribonucleic acid

SDS-PAGE: sodium dodecyl sulfate-polyacrylamide gel electrophoresis

SOD1: superoxide dismutase 1

TA: tibialis anterior

TDP-43: TAR DNA-binding protein 43

1. Introduction

1-1 Overview of amyotrophic lateral sclerosis (ALS)

Amyotrophic lateral sclerosis (ALS), or Lou Gehrig's disease, is a fatal neuromuscular disease characterized by the degeneration of upper and lower motor neurons, leading to muscle weakness, speech and swallowing disabilities, progressive paralysis, and ultimately respiratory failure (Paez-Colasante et al., 2015). It is the most common motor neurodegenerative disease, with an estimated incidence of 2–3 per 100,000 per year, and it is diagnosed most often between the ages of 40 and 60 years (Chiò et al., 2009). In Japan, 9950 patients received ALS-awarded certificates of financial aid for the treatment of a designated intractable disease at the end of the 2014 fiscal year (http://www.nanbyou.or.jp/entry/1356#p09, accessed January 9 2017). ALS can be either familial (~10%) or sporadic (~90%) and the majority of ALS patients die within 2–4 years of diagnosis (Kiernan et al., 2011). Previous studies have discovered ALS-related mutations in >30 genes, including *SOD1*, *TARDBP* (encoding TDP-43), *FUS*, *OPTN*, *VCP*, *UBQLN2*, *ERBB4*, and *C9ORF72* (DeJesus-Hernandez et al., 2011; Deng et al., 2011; Johnson et al., 2010; Kwiatkowski et al., 2009; Maruyama et al., 2010; Renton et al., 2011; Rosen et al., 1993; Sreedharan et al., 2008; Takahashi et al., 2013; Vance et al., 2009). The rate of discovery of ALS-related mutations is doubling every 4 years owing

to technological innovations, such as whole-exome analysis, whole-genome analysis, and genome-wide association studies (Al-chalabi et al., 2017). Recently, *NEK1* was identified as a new ALS gene in a whole-exome analysis (Kenna et al., 2016). However, the causal genetic factors in a large majority of ALS cases are still unknown (Taylor et al., 2016). Moreover, ALS is a multifactorial disease, and indeed many abnormalities have been identified as potential pathogenic factors in patients with ALS and animal models, including the accumulation of protein aggregates, defective RNA processing, oxidative stress, glutamate excitotoxicity, glial dysfunction, and abnormal muscle energy metabolism (Paez-Colasante et al., 2015; Zhu et al., 2015). This variation appears to be a roadblock to development of an effective therapy (Genç & Özdinler, 2014; Ittner et al., 2015). Currently, the glutamate release inhibitor riluzole and free radical scavenger edaravone are the only medications approved in Japan for ALS. Riluzole prolongs the life span of patients by a few months and edaravone modestly improves motor function (Abe et al., 2014; Lucette et al., 1996). Although many other drugs have been examined in clinical trials, including regenerative drugs, such as stem cell therapy, there remains a strong need for new treatment strategies for ALS (Ittner et al., 2015; Mazzini et al., 2016).

1-2 *SOD1-G93A* mouse model of ALS

In ~20% of familial cases of ALS, patients harbor a mutation in the gene encoding Cu/Zn superoxide dismutase 1 (SOD1) (Ittner et al., 2015; Paez-Colasante et al., 2015). Pathogenic gain-of-function *SOD1* mutations in ALS are associated with the propensity of mutant SOD1 to misfold, presenting a non-native structure (Silverman et al., 2016). Moreover, mice expressing human SOD1 (hSOD1) with the ALS-linked G93A mutation under the endogenous human *SOD1* promoter manifest progressive muscle paralysis, similar to that observed in clinical cases. In addition, although SOD1-G93A mice lack TDP-43 aggregation in motor neurons, a pathology observed in 97% of ALS cases, they do exhibit many, if not all, histopathological hallmarks of familial and sporadic ALS, including muscle atrophy and a loss of motor neurons (Gurney et al., 1994; Ittner et al., 2015; Zhu et al., 2015). Moreover, SOD1-G93A mice show short life span, which ease us to evaluate the effect of a candidate drug or method on their survival. Based on these pathological features, these mice are widely used as models of ALS (Duan, 2016; Hocquemiller et al., 2016). Several ALS-linked SOD1 mutations other than G93A have been used to generate transgenic mouse models of SOD1-linked ALS, including G37R, H46R, G85R, D90A, and G127X (Zhu et al., 2015), but these SOD1-linked ALS models have not been characterized as extensively as SOD1-G93A mice. In addition, other mouse models of ALS, including *C9ORF72*- or *TARDBP*-linked ALS, have recently been generated (Arnold et al., 2013; Liu et al., 2016). However, compared with SOD1-G93A

mice, these models show long life spans and large individual differences in symptoms and disease progression.

1-3 Disease progression mechanisms of ALS

Based on studies of ALS patients and ALS model mice, three disease progression models have been proposed: the “dying-forward” hypothesis, “dying-back” hypothesis, and “independent neurodegeneration” hypothesis (Fig. 1). The “dying-forward” hypothesis proposes that ALS is mainly a disorder of cortico-motoneurons, which connect monosynaptically with anterior horn cells, mediating anterograde degeneration of anterior horn cells via glutamate-mediated excitotoxicity (Geevasinga et al., 2016; Kiernan et al., 2011). The neurotransmitter glutamate conveys nerve signals from upper motor neurons to lower motor neurons by binding to ionotropic glutamate receptors, which are classified into three groups, *N*-methyl-D-aspartate (NMDA), α-amino-3-hydroxy-5-methyl-4-isoxazolepropionic acid (AMPA), and kainite receptors (Meldrum, 2000). In the ALS pathogenesis, NMDA and AMPA receptors seem to be important (Jaiswal, 2014; Spalloni et al., 2013). Abnormal activation of these receptors results in an increased influx of Na^+ and Ca^{2+} ions, leading to glutamate-mediated excitotoxicity. The alteration of NMDA receptor properties, increases in bursting activity, and neuronal hyperexcitability have been reported in the spinal interneurons of ALS model mice (Jiang

et al., 2009). Indeed, morphological and functional changes within cortico-motoneurons at the presymptomatic stage and neuronal hyperexcitability at the embryonic stage were observed in mouse models (Kuo et al., 2004; Pieri et al., 2009). In addition, increased expression of Ca^{2+}-permeable AMPA receptors resulting from an RNA editing defect of the pre-mRNA of GluA2, an AMPA receptor subunit, has been detected in motor neurons derived from ALS patients (Kwak & Kawahara, 2005; Takuma et al., 1999). It was also reported that the defects in GluA2 editing are caused by decreases in Adenosine Deaminase Acting on RNA 2 (ADAR2) RNA editing enzyme activity, and ADAR2 knockout mice show ALS-like phenotypes, including TDP-43 aggregation in motor neurons (Yamashita et al., 2013).

By contrast, the "dying-back" hypothesis proposes that motor neuron degeneration first becomes evident as a size reduction of motor nerve terminals and subsequent denervation at neuromuscular junctions (NMJs), cholinergic synapses essential for the motoneural control of muscle contraction (see Chapter 1-5) (Fig. 2) (Dadon-Nachum et al., 2011; Fischer et al., 2004; Murray et al., 2010; Valdez et al., 2012). Motor neuron degeneration then progresses proximally. In addition, some researchers have proposed the "independent neurodegeneration" hypothesis, in which upper motor neurons and lower neurons degenerate independently, perhaps in a stochastic manner (Ravits et al., 2007).

Despite extensive studies of this disease, the exact mechanism of ALS development and progression is still largely unknown. In particular, the connection between the "dying-forward" hypothesis and "dying-back" hypothesis remains entirely uncertain. Nevertheless, because the "dying-back" pathology is observed not only in ALS model mice, but also in ALS patients based on autopsy or electrophysiology results (Bruneteau et al., 2013; Dadon-Nachum et al., 2011; Fischer et al., 2004), NMJ protection might be an effective treatment. However, there is no promising NMJ-targeted therapy for ALS.

1-4 Guideline for pre-clinical studies in ALS

Despite many preclinical studies since the development of ALS model mice, the majority of beneficial effects observed have not translated to humans (Genç & Özdinler, 2014; Ittner et al., 2015). Minocycline is a notable failure. This antibiotic showed anti-apoptotic and anti-inflammatory effects and resulted in a prolonged lifespan in ALS model mice when administered before disease onset (Zhu et al., 2002). However, in clinical trials, minocycline worsened ALS symptoms compared with a placebo (Gordon et al., 2007). The failure to translate positive drug testing results in mouse models to humans has been attributed, at least in part, to methodological faults, rather than to problems with the models themselves. Thus, in order to improve the effectiveness of mouse models and the design of preclinical experiments, a strict guideline for preclinical

ALS studies was established by the European ALS/NMD group. Following this guideline is strongly recommended to improve the translation of results to humans (Ludolph et al., 2010). In fact, minocycline did not have beneficial effects on the survival of ALS model mice in a preclinical study that was in accordance with this guideline (Scott et al., 2008). Moreover, recent studies using experimental settings that fit this guideline have reported that even riluzole and other drugs previously reported to enhance survival in ALS model mice failed to exhibit efficacy in ALS mice (Jablonski et al., 2014; Scott et al., 2008).

1-5 Overview of the neuromuscular junction (NMJ) and Dok-7

In mammalian NMJs, the neurotransmitter acetylcholine (ACh) is released from the presynaptic motor nerve terminal and binds to densely clustered nicotinic ion-channel ACh receptors (AChRs) on the postsynaptic muscle membrane (Fig. 2). The binding of ACh to AChR depolarizes the muscle membrane and induces action potentials, leading to muscle contraction (Sanes & Lichtman, 1999). The formation and maintenance of NMJs are orchestrated by the muscle-specific receptor tyrosine kinase (MuSK) and agrin, the extracellular MuSK activator released by motor neurons. Agrin activates MuSK by binding to the MuSK co-receptor Low density lipoprotein receptor-related protein 4 (Lrp4) (Kim & Burden, 2008; Zhang et al., 2008). In addition to agrin and Lrp4, the activation of MuSK requires the muscle protein Downstream of tyrosine kinases-7 (Dok-

7) as an essential cytoplasmic activator (Hamuro et al., 2008; Inoue et al., 2009; Okada et al., 2006). Our laboratory previously demonstrated that Dok-7 directly interacts with the cytoplasmic portion of MuSK and activates the receptor kinase (Inoue et al., 2009). Like mice lacking MuSK, Dok-7-deficient mice form no NMJs during embryonic development and exhibit neonatal death due to respiratory failure (Okada et al., 2006). In addition, postnatal knockdown of *dok-7* gene expression in mice reduces the size of NMJs and impairs motor function (Eguchi et al., 2016). Moreover, recessive loss- or reduction-of-function mutations in the human *DOK7* gene underlie *DOK7* myasthenia, a limb-girdle type of congenital myasthenic syndrome characterized by NMJs that are about half the normal size (Beeson et al., 2006; Hamuro et al., 2008; Palace et al., 2007). Dok-7 knock-in mice (*DOK7* myasthenia model mice), which are homozygous for the most frequent frameshift mutation in *DOK7* myasthenia patients, show abnormally small NMJs and die within 3 weeks (Arimura et al., 2014). These findings strongly indicate that Dok-7 is crucial for the formation and maintenance of NMJs throughout life, although the precise mechanisms of Dok-7-mediated MuSK activation are not fully established. On the other hand, enhanced MuSK activation and NMJ formation are prominently observed in transgenic mice that overexpress Dok-7 specifically in the skeletal muscle under the control of the human skeletal α-actin (HSA) promoter (Arimura et al., 2014; Inoue et al., 2009). These results suggest that enhanced NMJ formation by the forced expression of

Dok-7 in the muscle could alleviate not only *DOK7* myasthenia, but also a variety of neuromuscular disorders associated with an NMJ synaptopathy.

1-6 *DOK7* gene therapy for neuromuscular diseases

To investigate whether the forced expression of Dok-7 benefits neuromuscular disorders with defects in NMJ formation, our laboratory previously generated a viral vector carrying the human *DOK7* gene. Adeno-associated virus (AAV), a non-enveloped virus that packages a linear single-stranded DNA genome, was used for this experiment owing to its non-pathogenic nature and its previous use in clinical studies for gene therapy. The tissue specificity of AAV is determined by the capsid serotype; 12 major serotypes (AAV1–12) have been identified in humans and non-human primates (Daya & Berns, 2008; Mietzsch et al., 2014). Since AAV9 efficiently targets muscle after systemic injection (Katwal et al., 2013; Zincarelli et al., 2008), serotype 9 has been used in preclinical studies of neuromuscular diseases (Duan, 2016; Hocquemiller et al., 2016). Based on these findings, our laboratory generated AAV-D7, an AAV serotype 9 vector carrying the human *DOK7* gene tagged with enhanced green fluorescent protein (EGFP) under the control of the cytomegalovirus (CMV) promoter, which displays higher activity in skeletal muscle than that of the HSA promoter (Arimura et al., 2014; Hagstrom et al., 2000). As expected, systemic administration of AAV-D7 results in the activation of MuSK

and enlargement of NMJs in wild-type mice. Moreover, the administration of AAV-D7 after disease onset, i.e., *DOK7* gene therapy, enlarges NMJs and enhances motor activity and life span in *DOK7* myasthenia model mice (Arimura et al., 2014). Furthermore, this therapy also enlarges NMJs and enhances motor activity and life span in a mouse model of autosomal dominant Emery-Dreifuss muscular dystrophy (AD-EDMD), a disease associated with defective NMJs due to mutations in the lamin A/C gene (Arimura et al., 2014; Méjat et al., 2009). These observations demonstrate the potential for *DOK7* gene therapy in myopathies with NMJ defects, but the effectiveness of this therapy in the treatment of other diseases accompanied by NMJ defects has not been proven.

2. Results

2-1 *DOK7* gene therapy suppresses motor nerve terminal degeneration at the NMJ in ALS mice

Previous studies have demonstrated the potential for *DOK7* gene therapy in myopathies with small NMJs, such as *DOK7* myasthenia and AD-EDMD (Arimura et al., 2014). I suspected that this therapy might also benefit motor neurodegenerative diseases with NMJ structural defects, such as ALS, because it enlarges NMJs, including presynaptic motor nerve terminals, which might counteract the size reduction and denervation of the terminal. Since motor nerve terminal defects appear to play an important role in the pathogenesis of ALS in both human patients and animal models (Bruneteau et al., 2015; Dadon-Nachum et al., 2011; Fischer et al., 2004; Murray et al., 2010; Valdez et al., 2012), I examined whether *DOK7* gene therapy ameliorates pathology in a mouse model of ALS.

In this study, I used C57BL/6 mice expressing human SOD1 (hSOD1) with the ALS-linked G93A mutation (hereafter, ALS mice) as a model of ALS because these mice show the hallmarks of familial and sporadic ALS, including NMJ defects (Dadon-Nachum et al., 2011; Zhu et al., 2015). To investigate the effect of AAV-D7 on ALS mice, I first intravenously administered 1.2×10^{12} viral genomes (vg) of AAV-D7 to male ALS mice at an early symptomatic stage (postnatal day 90, P90) (Kondo et al., 2014), and performed histological analyses 30 days later. The units “vg” indicate the number of virus particles

containing the viral genome. Note that the forelimb grip strengths of ALS mice in the control and AAV-D7 treatment groups were significantly weaker than that of wild-type mice at P84 (before treatment), confirming that these ALS mice were already at an early symptomatic stage (Fig. 3A). Additionally, I confirmed the h*SOD1-G93A* transgene copy number by real-time quantitative PCR owing to its potential to affect disease progression (Pérez-García & Burden, 2012). Transgene copy number was comparable in both groups of ALS mice (Fig. 3B). In these model mice, AAV-D7 treatment strongly enhanced MuSK activation, as judged by the phosphorylation of MuSK and AChR, the latter of which is triggered by the activation of MuSK (Fig. 4). To evaluate the effects of AAV-D7 on NMJ morphology, I analyzed fluorescently labeled NMJs in the diaphragm muscle by confocal microscopy because the diaphragm muscle is thin and allows for a comprehensive overview of the entire innervation pattern. Whole mounts of diaphragm muscle were stained with antibodies against synapsin-1, which is a neuron-specific protein that binds to synaptic vesicles and is localized in the motor nerve terminal (Hirokawa et al., 1989), and α-bungarotoxin (α-BTX), a snake neurotoxin, to label AChRs, which are concentrated in the postsynaptic membranes of skeletal muscle (DeChiara et al., 1996; Dellisanti et al., 2007). I found that AAV-D7 treatment significantly increased the area of motor nerve terminals at NMJs in the diaphragm muscle, together with the postsynaptic area characterized by clustered AChRs, indicating positive effects on motor neurons at 30

days post-infection (Fig. 5A, B, and C). Moreover, AAV-D7 treatment significantly increased the number of synapsin-1-positive AChR clusters, indicating that this treatment suppresses denervation at NMJs in ALS mice (Fig. 5D). These results demonstrated that *DOK7* gene therapy protected NMJs from nerve terminal degeneration in ALS mice. Note that AAV-D7 expresses human Dok-7 tagged with EGFP, and its infection could be monitored (Fig. 5A).

2-2 *DOK7* gene therapy suppresses muscle atrophy with no adverse effects on proximal motor neurons in ALS mice

NMJ defects are thought to be a cause of muscle atrophy in motor neuron diseases, including ALS (Bongers et al., 2013; Yoo & Ko, 2012). Thus, I further evaluated the effects of AAV-D7 treatment on muscle atrophy by analyzing muscle fiber size in tibialis anterior muscle. I found that both the cumulative percentage and mean fiber cross-section area showed significant improvement, indicating a beneficial effect of AAV-D7 treatment on muscle atrophy in ALS mice at 30 days after treatment (Fig. 6). In addition, to examine the effect of AAV-D7 treatment on progressive motor neuron death, another hallmark of ALS (Yoo & Ko, 2012), I subjected the ventral horns of the L4-L5 spinal cord segments to Nissl staining and counted the number of motor neuron cell bodies. Nissl staining can label the Nissl body, a large granular body found in neurons (Einarson, 1932). I found

that the number of motor neuron cell bodies was comparable in AAV-D7-treated and untreated ALS mice (Fig. 7). In addition, I visualized L4 ventral root axons by immunofluorescent staining using an anti-neurofilament-H antibody. Neurofilaments are the most abundant cytoskeletal component of the motor neuron. Similar to the results obtained for motor neuron number, proximal axon atrophy was not significantly affected by AAV-D7 treatment, as evidenced by the comparable distribution of L4 ventral root axons in the two groups (Fig. 8). Together, these data indicate that *DOK7* gene therapy suppressed nerve terminal degeneration at NMJs and muscle atrophy in ALS mice, with no obvious effects on proximal motor neuron degeneration at 30 days post-infection.

2-3 *DOK7* gene therapy prolongs life span in ALS mice

Since ALS in humans is usually diagnosed after the onset of symptoms (Zhu et al., 2015), I established the disease onset separately in each ALS mouse to examine the effects of *DOK7* gene therapy on life span. First, I set the reference points at P84 and P86, within an early symptomatic stage (Fig. 3A), to individually obtain a reference forelimb grip strength for each ALS mouse as the mean of those at P84 and P86. Then, the disease onset for each ALS mouse was defined as the point when its grip strength dropped to 80% or less of its own reference value for 2 consecutive days, since ALS mice sometimes show fluctuations of ~10%, even over 2 days. At this individually defined disease onset, I

intravenously administered AAV-D7 to each male ALS mouse. In the first trial, I administered 4×10^{11} vg of AAV-D7 to four male ALS mice, but only one of four ALS mice showed prolonged survival (Fig. 9). Thus, I administered a higher dose (1.2×10^{12} vg) of AAV-D7 into each male ALS mouse to perform a survival analysis according to the guidelines for pre-clinical ALS studies (Ludolph et al., 2010), which requires a minimum of 12 mice of a single gender and of comparable h*SOD1-G93A* transgene copy number for each test or control group. As mentioned above, this guideline was recently established to improve translation to humans, which was a major weakness of many previous clinical trials (Genç & Özdinler, 2014; Ludolph et al., 2010). Remarkably, even riluzole and other drugs reported to enhance the survival of ALS model mice failed to exhibit efficacy in ALS mice when tested in experimental settings that adhered to this guideline (Jablonski et al., 2014; Scott et al., 2008). However, *DOK7* gene therapy significantly prolonged not only life span, but also the duration of survival after onset (Fig. 10A and B). Neither age nor the grip strength at disease onset differed significantly between AAV-D7-treated and untreated mice (Fig. 10C and D). The h*SOD1-G93A* transgene copy number was comparable between these groups (Fig. 10E). In addition, I administered 1.2×10^{12} vg of AAV-EGFP to ALS mice after onset, which was individually defined by grip strength as described above. I confirmed that treatment with AAV-EGFP

did not alter the survival of ALS mice, showing that neither AAV infection nor EGFP expression had any obvious effect on survival (Fig. 11).

2-4 *DOK7* gene therapy improves motor activity in ALS mice

Interestingly, as AAV-EGFP-treated ALS mice entered the late-to-end stage of the disease, the contrast in spontaneous motor activity with AAV-D7-treated mice was striking (Fig. 12). Thus, I used the automated home cage behavioral system to measure stress-independent spontaneous motor activity (Hayworth & Gonzalez-Lima, 2009; Ludolph et al., 2010). This device consists of two square-shaped frames that deliver infrared rays into the space inside the square. The home cage was placed in the square to measure spontaneous activity. These data showed an increase in spontaneous activity resulting from AAV-D7 treatment throughout the test period and demonstrated that *DOK7* gene therapy significantly improves locomotor activity and speed compared with those of AAV-EGFP-treated mice at P155 (Fig. 13).

3. Discussion

Accumulating evidence demonstrates that defects in NMJs are associated with various types of neuromuscular disorders, including myasthenia, motor neuron degeneration, and

sarcopenia (i.e., age-related muscle atrophy) (Deschenes et al., 2010; Murray et al., 2010; Sleigh et al., 2014). For example, patients with ALS, including one carrying a *SOD1* mutation, manifest NMJ defects, even when biopsied at the early symptomatic stage (Bruneteau et al., 2015). Consistent with this, mouse models of ALS with *SOD1*, *TARDBP*, *FUS*, *UBQLN2*, or *C9ORF72* mutations also display NMJ defects (Arnold et al., 2013; Dadon-Nachum et al., 2011; Le et al., 2016; Liu et al., 2016; Sharma et al., 2016). In addition, mouse models of neurodegenerative diseases, including spinal muscular atrophy and Charcot-Marie-Tooth disease type 2D, show NMJ abnormalities (Murray et al., 2010; Sleigh et al., 2014). Furthermore, denervation at the NMJ occurs before myofiber atrophy in sarcopenia model mice and rats (Chung et al., 2016; Deschenes et al., 2010). Our laboratory previously demonstrated that *DOK7* gene therapy activates the muscle-specific kinase MuSK to enlarge NMJs, and ameliorates myopathies characterized by NMJ defects (*DOK7* myasthenia and AD-EDMD) in mouse models, suggesting its potential application to a range of neuromuscular diseases. However, the effectiveness of *DOK7* gene therapy in motor neuron diseases is not known. In this thesis, I demonstrated that single-dose administration of AAV-D7 at the symptomatic stage suppresses denervation at NMJs and improves muscle atrophy, with no obvious effects to motor neuron cell body loss or axon atrophy in ALS mice. Moreover, I confirmed that AAV-D7 treatment after individually defined disease onset improved life span and motor activity in ALS mice,

although the precise mechanisms by which *DOK7* gene therapy suppresses denervation at the NMJ and disease progression in ALS remain to be established.

ALS mice used in this study, transgenic mice expressing an ALS-linked mutant form of human SOD1, were generated in 1994 (Gurney et al., 1994). As mentioned above, they are widely used in pre-clinical studies owing to their phenotypic resemblance to familial and sporadic ALS patients, including progressive muscle weakness, motor neuron cell body loss, axon atrophy, and lethality. However, SOD1 mutations are only observed in 2% of all ALS cases (Rosen et al., 1993). Thus, it is important to evaluate whether *DOK7* gene therapy is effective in ALS model mice other than SOD1-ALS models (Arnold et al., 2013; Le et al., 2016; Liu et al., 2016). In addition, given that gender differences have been observed in the incidence, disease progression and treatment response in patients and animal models of ALS (Pollari et al., 2014), it is desirable to test the effects of *DOK7* gene therapy in female ALS mice.

A few studies have evaluated the effect of NMJ preservation on ALS patients and model mice. Genetic deletion of Nogo-A, an inhibitor of neurite outgrowth, delays denervation at NMJs and prolongs life span in ALS model mice (Jokic et al., 2006), though its effect on motor function has not been determined. Consistent with this, treatment with an anti-Nogo-A antibody improves muscle innervation and motor function in ALS model mice; however, its effect on survival has not been determined (Bros-Facer

et al., 2014). Moreover, therapeutic treatment with an anti-Nogo-A antibody (Ozanezumab) does not show any benefits for ALS patients according to a phase II clinical trial (Meininger et al., 2017). Interestingly, a transgene that modestly increases the muscle-specific expression of MuSK from the embryonic stage delayed denervation at NMJs and improved motor function, but failed to increase the survival of ALS mice (Pérez-García & Burden, 2012). Nevertheless, the effect of ectopic MuSK expression induced after disease onset is not known, and high MuSK expression in the muscle has been shown to induce scattered NMJ formation throughout myofibers and to cause severe muscle weakness (Kim & Burden, 2008), suggesting that forced MuSK expression is not suitable as a therapeutic method. By contrast, *DOK7* gene therapy greatly facilitates NMJ enlargement in the appropriate central region of myofibers without lethal effects for more than 1 year in *DOK7* myasthenia model mice (Arimura et al., 2014), suggesting that *DOK7* gene therapy is a safer therapeutic approach.

Previous studies have shown that degeneration of motor nerve terminals at NMJs occurs independently of motor neuron cell death. The deletion of the pro-apoptotic protein BAX suppresses motor neuron cell death, but fails to prevent denervation at NMJs in ALS model mice (Gould et al., 2006). In addition, the deletion of Cyclophilin D, a key positive regulator of the mitochondrial permeability transition (Baines et al., 2005), in three lines of SOD1-linked ALS model mice suppresses motor neuron cell death, but does

not affect denervation at NMJs, motor axon degeneration, disease progression, and survival (Parone et al., 2013). On the other hand, I show here that *DOK7* gene therapy suppressed denervation at NMJs in ALS mice, with no obvious effects on motor neuron cell death. Therefore, although I demonstrate in this study that *DOK7* gene therapy by itself benefits ALS as an NMJ-targeting therapy, this therapy could be more effective when used in combination with therapies aimed at promoting motor neuron survival.

As mentioned above, the precise mechanisms by which *DOK7* gene therapy suppresses denervation at the NMJ in ALS remain to be determined. It is likely that the mechanism involves a retrograde signal(s) from the skeletal muscle to the motor neuron that is evoked by Dok-7-mediated MuSK activation. This idea is consistent with the enlarged nerve terminals at NMJs observed in Dok-7 transgenic mice that overexpress Dok-7 specifically in the skeletal muscle as well as in AAV-D7-treated mice. Several studies have evaluated retrograde signals at NMJs. The MuSK co-receptor Lrp4 functions as an agrin receptor, but also acts as a retrograde signal from the muscle and organizes presynaptic differentiation during embryonic NMJ formation (Yumoto et al., 2012). Fibroblast growth factor (FGF) 7/10/22, lamininβ2, and collagen α4 are other muscle-derived presynaptic organizers in NMJ formation and maintenance (Fox et al., 2007). Glial-derived neurotrophic factor (GDNF) is a muscle-derived motor neuron survival factor and facilitates NMJ maturation (Kanning et al., 2010). Interestingly, in an in vitro NMJ co-

culture system that separates motor neuron cell bodies from their axons and NMJs, GDNF exerts anti-apoptotic effects on the motor neuron when it is locally applied to the NMJ side, but not when it is applied to the cell body side (Zahavi et al., 2015). In addition, fibroblast growth factor binding protein 1 (FGFBP1), a secreted protein that functions to chaperone FGF ligands from the extracellular matrix to cognate receptors, is secreted from muscle fibers and is concentrated at NMJs (Abuharbeid et al., 2006; Tassi et al., 2007; Wu et al., 1991). Interestingly, its expression level decreases prior to NMJ degeneration during aging and in ALS model mice. Moreover, genetic deletion of FGFBP1 in ALS model mice accelerates degeneration at NMJs and shortens life span (Taetzsch et al., 2017). Uncovering the precise mechanism by which Dok-7-mediated MuSK activation suppresses denervation at NMJs would not only clarify the therapeutic mechanism of AAV-D7 treatment, but would also deepen our understanding of ALS pathology and pave the way toward finding new therapeutic targets for ALS.

In this thesis, I establish proof-of-concept that *DOK7* gene therapy has potential as treatment for various motor neuron diseases that manifest NMJ defects, either alone or in combination with other therapies, as discussed above. AAV-D7 in this study expresses Dok-7 tagged with EGFP under the control of the CMV promoter with high transcriptional activity, but low tissue specificity. Thus, the construct of AAV-D7 needs to be optimized for further clinical trials (for instance, the use of a muscle-specific

promoter). Pharmacological enlargement of NMJs might also be a useful therapy for motor neuron diseases.

4. Materials and methods

4-1 Mice

The animal studies were performed in accordance with the University of Tokyo guidelines for animal care and use, and approved by the institutional animal care and use committee. Transgenic mice expressing human *SOD1* (h*SOD1*) with the ALS-linked G93A mutation (B6. Cg-Tg [SOD1-G93A] 1Gur/J, Stock No. 004435) were purchased from the Jackson Laboratory (Bar Harbor, ME, USA) and bred on the C57BL/6J background, and male mice were used in this study. Mice were genotyped by PCR using mouse genomic DNA as the template. Mouse genomic DNA was isolated by incubating mouse ear biopsies in lysis buffer containing proteinase K [50 mM Tris-HCl (pH 8.0), 20 mM EDTA (pH 8.0), 0.1 M NaCl, 1% sodium dodecyl sulfate, and proteinase K (0.2 mg/ml)], followed by extraction with phenol/chloroform/isoamyl alcohol (25:24:1). GoTaq DNA polymerase (Promega, Madison, WI, USA) was used for DNA amplification. Specific primers for h*SOD1-G93A* and internal positive control (*Il2*) sequences were as follows (5′ to 3′):

CATCAGCCCTAATCCATCTGA (h*SOD1-G93A*, forward), CGCGACTAACAATCAAAGTGA (h*SOD1-G93A,* reverse), CTAGGCCACAGAATTGAAAGATCT (*Il2*, forward), and GTAGGTGGAAATTCTAGCATC TCC (*Il2*, reverse). The PCR conditions were as

follows: 1 cycle of 95°C for 3 min, followed by 35 cycles of 95°C for 30 s and annealing at 60°C for 30 s using the GeneAmp 9700 PCR System Thermocycler (Applied Biosystems, Foster City, CA, USA). Mice were housed on a 12/12-h light-dark cycle in specific pathogen-free conditions with free access to water and standard mouse chow in the animal facility of the Institute of Medical Science, the University of Tokyo.

4-2 Evaluation of h*SOD1-G93A* transgene copy number

Differences in transgene copy number were estimated by real-time quantitative PCR; differences were quantified as the difference in cycle threshold (ΔCt) between the transgene (h*SOD1-G93A*) and a reference gene (mouse *apob*), according to the procedure recommended by the Jackson Laboratory. SYBR Premix Ex Taq II (Takara Bio, Shiga, Japan) was used for the real-time amplification of DNA. Specific primers for h*SOD1-G93A* and *apob* sequences were as follows (5′ to 3′): GGGAAGCTGTTGTCCCAAG (h*SOD1-G93A*, forward), CAAGGGGAGGTAAAAGAGAGC (h*SOD1-G93A*, reverse), CACGTGGGCTCCAGCATT (*apob*, forward), and TCACCAGTCATTTCTGCCTTTG (*apob*, reverse). The PCR conditions were as follows: 1 cycle of 95°C for 10 min, followed by 40 cycles of 95°C for 15 s and annealing at 60°C for 1 min using the CFX Connect Real-time System (Bio-Rad Laboratories, Hercules, CA, USA).

4-3 AAV production

The cDNA encoding EGFP or human Dok-7 cDNA tagged with EGFP was cloned into pAAV-MCS (Agilent Technologies, Santa Clara, CA, USA), which carries the cytomegalovirus promoter, to obtain the pAAV-EGFP or pAAV-Dok-7-EGFP plasmid (Arimura et al., 2014). Plasmids were expanded in *Escherichia coli* DH5α and prepared using the Endotoxin-free Plasmid Giga-prep Kit (Qiagen, Valencia, CA, USA) or NucleoBond PC 10000 EF Endotoxin-free Plasmid DNA Purification Kit (Machery-Nagel, Düren, Germany) according to the supplier's protocol. For the production of AAV-EGFP or AAV-D7, HEK293T or HEK293EB cells were co-transfected with the AAV9 chimeric helper plasmid pRep2Cap9, the adenovirus helper plasmid pHelper (Agilent Technologies), and pAAV-EGFP or pAAV-Dok-7-EGFP in a CellBIND Surface HYPERFlask M Cell Culture Vessel (Corning, Corning, NY, USA) using polyethyleneimine and cultured for 5 days (Lin et al., 2007; Matsushita et al., 2004). The AAV particles were purified by CsCl or iodixanol density-gradient ultracentrifugation using the Himac CP80WX (Hitachi Koki, Tokyo, Japan) with a P40ST rotor (Hitachi Koki) (145,000 × *g*, 42 h, 21°C) or Optima XE-90 Ultracentrifuge (Beckman Coulter Inc., Miami, FL, USA) with a VTi 50 rotor (Beckman Coulter Inc.) (125,504 × *g*, 15 h 16 min, 16°C) (Tomono et al., 2016). The viral titers (vg) were determined by real-time

quantitative PCR using the AAVpro Titration Kit (Takara Bio) and the CFX Connect Real-time System (Bio-Rad Laboratories) with specific primers for the *EGFP* sequence as follows (5′ to 3′): GTGAGCAAGGGCGAGGAG (forward) and GTGGTGCAGATGAACTTCAGG (reverse).

4-4 Intravenous injection of AAV-D7

Either 4×10^{11} vg or 1.2×10^{12} vg of AAV-D7 or 1.2×10^{12} vg of AAV-EGFP was intravenously injected by a single shot via the tail vein at the symptomatic stage (P90) or after the individually defined disease onset.

4-5 Immunoprecipitation and immunoblotting

Whole tissue lysates (WTLs) were prepared from the hind-limb muscle with alkaline lysis buffer [50 mM Tris-HCl (pH 9.5), 1% sodium deoxycholate, protease inhibitors (Complete, Roche, Basel, Switzerland), and phosphatase inhibitors (PhosSTOP; Roche)]. For immunoprecipitation, WTLs were incubated with antibodies against MuSK (C-19 and N-19) or AChRβ1 (H-101) (Santa Cruz Biotechnology, Santa Cruz, CA, USA), followed by incubation with protein G-Sepharose (GE Healthcare, Milwaukee, WI, USA). For immunoblotting, immunoprecipitates or WTLs were subjected to SDS-PAGE and transferred to a polyvinylidene fluoride (PVDF) microporous membrane (Merck

Millipore, Billerica, MA, USA). The membranes were blocked with Blocking-One P (Nacalai Tesque, Kyoto, Japan) and then probed with primary antibodies against phosphotyrosine (4G10) (Merck Millipore), Dok-7 (A-7), AChRβ1 (H-101) (Santa Cruz Biotechnology), MuSK (AF562) (R&D Systems, Minneapolis, MN, USA), hSOD1 (#2770), or GAPDH (#2118) (Cell Signaling Technology, Beverly, MA, USA), followed by incubation with secondary horseradish peroxidase-labeled anti-mouse IgG (GE Healthcare), anti-rabbit IgG (GE Healthcare), anti-goat IgG (Santa Cruz Biotechnology), or TrueBlot anti-rabbit IgG antibodies (Rockland, Gilbertsville, PA, USA). The blots were visualized using a LAS4000 Imager with ECL Prime Western Blotting Detection Reagent (GE Healthcare). Molecular weight (kDa) was estimated using Precision Plus Protein All Blue Standards (Bio-Rad Laboratories).

4-6 Whole-mount staining of NMJs

Diaphragm muscles were fixed in 1% paraformaldehyde (PFA) in phosphate-buffered saline (PBS) overnight at 4°C and then rinsed with PBS. The muscles were permeabilized with 1% Triton X-100 and 2% BSA in PBS, and incubated with anti-synapsin-1 (#5297) rabbit monoclonal antibodies (Cell Signaling Technology) followed by incubation with Alexa 647-conjugated anti-rabbit IgG (Thermo Scientific, Bremen, Germany) and Alexa 594-conjugated α-BTX (Thermo Scientific). Stained muscles were mounted with

VECTORSHIELD H-1400 (Vector Laboratories, Inc., Burlingame, CA, USA). Confocal Z serial images were obtained using an FV1000 Confocal Laser Scanning Microscope (Olympus, Tokyo, Japan) and collapsed into a single image. The size (area) and number of presynaptic motor nerve terminals and postsynaptic AChR clusters were quantified using cellSens Digital Imaging Software (Olympus). For quantification, 7 microscopic fields with a 20× objective were chosen at random on the diaphragm muscle from each mouse, and 170–260 synaptic sites were analyzed per mouse. These experiments were conducted in a blinded fashion.

4-7 Quantification of myofiber size

Tibialis anterior (TA) muscles were fixed in 4% PFA in PBS and dehydrated, cleared, and embedded in paraffin wax (Sakura Finetek, Tokyo, Japan). Transverse sections of TA muscle were prepared at a thickness of 7 μm using a Leica RM2125 Rotary Microtome (Leica Microsystems, Wetzlar, Germany) and subjected to hematoxylin and eosin (H&E) staining. Bright-field images of muscle bundles were obtained using a BioREVO fluorescent microscope (Keyence, Osaka, Japan). The cross-section area of the TA muscle fiber was measured using cellSens Digital Imaging Software. For quantification, at least 450 myofibers per mouse were analyzed. These experiments were conducted in a blinded fashion.

4-8 Quantification of motor neuron number

Mice were transcardially perfused with 4% PFA in PBS under deep isoflurane anesthesia. The spinal cord lumbar region was excised, postfixed overnight in 4% PFA in PBS, and then dehydrated, cleared, and embedded in paraffin wax (Sakura Finetek). Transverse sections of the L4-L5 spinal segment were prepared at a thickness of 5 μm using a Leica RM2125 rotary microtome and stained with Cresyl violet (Nissl staining) (2.9 mM Cresyl violet, 10 mM sodium acetate, pH 3.4) at 56°C for 90 min. Bright-field images of spinal cord sections were collected using a BioREVO fluorescent microscope. The number of motor neurons in the ventral horn was counted using cellSens Digital Imaging Software, and at least 29 sections were counted per mouse. The following criteria were used to count motor neuron cell bodies (Cai et al., 2015): (1) cells located in the anterior horn and (2) cells with a maximum diameter of 20 μm or more. These experiments were conducted in a blinded fashion.

4-9 Quantification of motor axon diameter

Mice were transcardially perfused with 4% PFA in PBS under deep isoflurane anesthesia. The L4 ventral roots were excised from spinal cord, and L4 ventral roots were then embedded in Tissue-tek O.C.T. Compound (Sakura Finetek) and frozen in cold isopentane.

Frozen tissue blocks were stored at -80°C. Transverse sections of 5 μm thick were prepared from L4 ventral roots at -20°C using a Leica Cryostat (model CM3050), airdried for 5 min, and fixed with cold acetone for 15 min. The tissues were then blocked with 5% goat serum for 1 h, followed by incubation with the anti-neurofilament-H rabbit polyclonal antibodies (AB1991) (Merck Millipore) at a dilution of 1:1,000 for 2 h at room temperature. They were then incubated with Alexa 594-conjugated goat anti-rabbit IgG (Thermo Scientific) at a dilution of 1:2,000 for 1 h at room temperature. Sections were mounted with VECTORSHIELD H-1400. Images were collected with a BioREVO fluorescent microscope. Axonal diameters of L4 roots were measured using cellSens Digital Imaging Software. These experiments were conducted in a blinded fashion.

4-10 Grip strength test and onset definition

The forelimb grip strength of each mouse was measured using a computerized electronic pull-strain gauge 1027DSM (Columbus Instruments, Columbus, OH, USA) as described previously (Eguchi et al., 2016). Five measurements were obtained per mouse, and the mean of these five measurements was used for statistical analyses. These experiments were conducted in a blinded fashion. To individually define disease onset, the reference forelimb grip strength for each ALS mouse was set as the mean of its strength values at P84 and P86. The onset was defined at the point when its grip strength dropped to 80%

or less of its own reference strength for 2 consecutive days. The forelimb grip strength of each mouse was measured every 2 days, unless two consecutive-day measurements were required to define the onset.

4-11 Open field test

Spontaneous motor activity was monitored using the IR Actimeter system (Panlab/Harvard Apparatus, Barcelona, Spain). For each measurement, a mouse was placed in the test cage (155 × 245 × 148 mm) for 5 min without recording in order to avoid any bias due to stress. Then, its movement was automatically recorded for 10 min by infra-red capture. We analyzed locomotor activity (counts) and mean speed (cm/s) using ActiTrack software (Panlab/Harvard Apparatus). These experiments were conducted in a blinded fashion.

4-12 Statistical analysis

Data were analyzed using JMP Pro 12 (SAS Institute Inc.) or Easy R software. Values are presented as means ± s.e.m. or ± s.d. Statistical differences between two groups were determined using the two-tailed Student's *t*-test for normally distributed data with comparable variances. The Kolmogorov–Smirnov test was used for comparisons of two cumulative curves. Data sets containing more than two groups were tested using analyses

of variance (ANOVA) and Bonferroni or Dunnett's *post-hoc* test. The nonparametric Mann–Whitney U test was used for data that were not normally distributed or when a normality test could not be applied. Statistical differences in cumulative survival were determined using the log-rank test. $P < 0.05$ was considered statistically significant.

5. References

Abe, K., Itoyama, Y., Sobue, G., Tsuji, S., Aoki, M., Doyu, M., Hamada, C., Kondo, K., Yoneoka, T., Akimoto, M., & Yoshino, H. (2014). Confirmatory double-blind, parallel-group, placebo-controlled study of efficacy and safety of edaravone (MCI-186) in amyotrophic lateral sclerosis patients. *Amyotroph. Lateral Scler. Frontotemporal Degener.* **15**, 610–617.

Abuharbeid, S., Czubayko, F., & Aigner, A. (2006). The fibroblast growth factor-binding protein FGF-BP. *Int. J. Biochem. Cell Biol.* **38**, 1463–1468.

Al-chalabi, A., Berg, L.H. Van Den, & Veldink, J. (2017). Gene discovery in amyotrophic lateral sclerosis: implications for clinical management. *Nat. Rev. Neurol.* **13**, 96–104.

Arimura, S., Okada, T., Tezuka, T., Chiyo, T., Kasahara, Y., Yoshimura, T., Motomura, M., Yoshida, N., Beeson, D., & Yamanashi, Y. (2014). *DOK7* gene therapy benefitsmouse models of diseases characterized by defects in the neuromuscular junction. *Science* **345**, 1505–1508.

Arnold, E.S., Ling, S.-C., Huelga, S.C., et al. (2013). ALS-linked TDP-43 mutations produce aberrant RNA splicing and adult-onset motor neuron disease without aggregation or loss of nuclear TDP-43. *Proc. Natl. Acad. Sci.* **110**, E736–E745.

Baines, P.C., Kaiser, A.R., Purcell, H.N., Blair, N.S., Osinska, H., Hambleton, A.M.,

Brunskill, W.E., Sayen, M.R., Gottlieb, A.R., Dorn, W.G., Robbins, J., & Molkentin, J.D. (2005). Loss of cyclophilin D reveals a critical role for mitochondrial permeability transition in cell death. *Nature* **434**, 658–662.

Beeson, D., Higuchi, O., Palace, J., et al. (2006). Dok-7 mutations underlie a neuromuscular junction synaptopathy. *Science* **313**, 1975–1978.

Bongers, K.S., Fox, D.K., Ebert, S.M., Kunkel, S.D., Dyle, M.C., Bullard, S. a, Dierdorff, J.M., & Adams, C.M. (2013). Skeletal muscle denervation causes skeletal muscle atrophy through a pathway that involves both Gadd45a and HDAC4. *Am. J. Physiol. Endocrinol. Metab.* **305**, E907-915.

Bros-Facer, V., Krull, D., Taylor, A., Dick, J.R.T., Bates, S.A., Cleveland, M.S., Prinjha, R.K., & Greensmith, L. (2014). Treatment with an antibody directed against nogo-a delays disease progression in the $SOD1^{G93A}$ mouse model of Amyotrophic lateral sclerosis. *Hum. Mol. Genet.* **23**, 4187–4200.

Bruneteau, G., Simonet, T., Bauché, S., et al. (2013). Muscle histone deacetylase 4 upregulation in amyotrophic lateral sclerosis: Potential role in reinnervation ability and disease progression. *Brain* **136**, 2359–2368.

Bruneteau, G., Bauché, S., Gonzalez de Aguilar, J.L., et al. (2015). Endplate denervation correlates with Nogo-A muscle expression in amyotrophic lateral sclerosis patients. *Ann. Clin. Transl. Neurol.* **2**, 362–372.

Cai, M.D., Choi, S.M., & Yang, E.J. (2015). The effects of bee venom acupuncture on the central nervous system and muscle in an animal hSOD1^{G93A} mutant. *Toxins (Basel).* **7**, 846–858.

Chiò, A., Mora, G., Calvo, A., Mazzini, L., Bottacchi, E., & Mutani, R. (2009). Epidemiology of ALS in Italy: a 10-year prospective population-based study. *Neurology* **72**, 725–731.

Chung, T., Park, J.S., Kim, S., Montes, N., Walston, J., & Höke, A. (2016). Evidence for dying-back axonal degeneration in age-associated skeletal muscle decline. *Muscle Nerve* **55**, 894–901.

Dadon-Nachum, M., Melamed, E., & Offen, D. (2011). The "dying-back" phenomenon of motor neurons in ALS. *J. Mol. Neurosci.* **43**, 470–477.

Daya, S., & Berns, K.I. (2008). Gene therapy using adeno-associated virus vectors. *Clin. Microbiol. Rev.* **21**, 583–593.

DeChiara, T.M., Bowen, D.C., Valenzuela, D.M., et al. (1996). The receptor tyrosine kinase MuSK is required for neuromuscular junction formation in vivo. *Cell* **85**, 501–512.

DeJesus-Hernandez, M., Mackenzie, I.R., Boeve, B.F., et al. (2011). Expanded GGGGCC hexanucleotide repeat in noncoding region of *C9ORF72* causes chromosome 9p-linked FTD and ALS. *Neuron* **72**, 245–256.

Dellisanti, C.D., Yao, Y., Stroud, J.C., Wang, Z.-Z., & Chen, L. (2007). Crystal structure of the extracellular domain of nAChR a1 bound to a-bungarotoxin at 1.94 Å resolution. *Nat. Neurosci.* **10**, 953–962.

Deng, H.-X., Chen, W., Hong, S.-T., et al. (2011). Mutations in *UBQLN2* cause dominant X-linked juvenile and adult-onset ALS and ALS/dementia. *Nature* **477**, 211–215.

Deschenes, M.R., Roby, M.A., Eason, M.K., & Harris, M.B. (2010). Remodeling of the neuromuscular junction precedes sarcopenia related alterations in myofibers. *Exp. Gerontol.* **45**, 389–393.

Duan, D. (2016). Systemic delivery of adeno-associated viral vectors. *Curr. Opin. Virol.* **21**, 16–25.

Eguchi, T., Tezuka, T., Miyoshi, S., & Yamanashi, Y. (2016). Postnatal knockdown of *dok-7* gene expression in mice causes structural defects in neuromuscular synapses and myasthenic pathology. *Genes to Cells* **21**, 670–676.

Einarson, L. (1932). A Method for Progressive Selective Staining of Nissl and Nuclear Substance in Nerve Cells. *Am. J. Pathol.* **8**, 295–308.

Fischer, L.R., Culver, D.G., Tennant, P., Davis, A.A., Wang, M., Castellano-Sanchez, A., Khan, J., Polak, M.A., & Glass, J.D. (2004). Amyotrophic lateral sclerosis is a distal axonopathy: evidence in mice and man. *Exp. Neurol.* **185**, 232–240.

Fox, M.A., Sanes, J.R., Borza, D.B., et al. (2007). Distinct Target-Derived Signals Organize Formation, Maturation, and Maintenance of Motor Nerve Terminals. *Cell* **129**, 179–193.

Geevasinga, N., Menon, P., Özdinler, P.H., Kiernan, M.C., & Vucic, S. (2016). Pathophysiological and diagnostic implications of cortical dysfunction in ALS. *Nat. Rev. Neurol.* **12**, 651–661.

Genç, B., & Özdinler, P.H. (2014). Moving forward in clinical trials for ALS: motor neurons lead the way please. *Drug Discov. Today* **19**, 441–449.

Gordon, P.H., Moore, D.H., Miller, R.G., et al. (2007). Efficacy of minocycline in patients with amyotrophic lateral sclerosis: a phase III randomised trial. *Lancet Neurol.* **6**, 1045–1053.

Gould, T.W., Buss, R.R., Vinsant, S., Prevette, D., Sun, W., Knudson, C.M., Milligan, C.E., & Oppenheim, R.W. (2006). Complete dissociation of motor neuron death from motor dysfunction by Bax deletion in a mouse model of ALS. *J. Neurosci.* **26**, 8774–8786.

Gurney, E.M., Pu, H., Chiu, Y.A., Dal Canto, C.M., Polchow, Y.C., Alexander, D.D., Caliendo, J., Hentati, A., Kwon, W.Y., Deng, H.-X., Chen, W., Zhai, P., Sufit, L.R., & Siddique, T. (1994). Motor neuron degeneration in mice that express a human Cu,Zn superoxide dismutase mutation. *Science* **264**, 1772–1775.

Hagstrom, J.N., Couto, L.B., Scallan, C., Burton, M., Mccleland, M.L., Fields, P.A., Arruda, V.R., Herzog, R.W., & High, K.A. (2000). Improved muscle-derived expression of human coagulation factor IX from a skeletal actin / CMV hybrid enhancer / promoter. **95**, 2536–2542.

Hamuro, J., Higuchi, O., Okada, K., Ueno, M., Iemura, S.I., Natsume, T., Spearman, H., Beeson, D., & Yamanashi, Y. (2008). Mutations causing *DOK7* congenital myasthenia ablate functional motifs in Dok-7. *J. Biol. Chem.* **283**, 5518–5524.

Hayworth, C.R., & Gonzalez-Lima, F. (2009). Pre-symptomatic detection of chronic motor deficits and genotype prediction in congenic B6.SOD1^{G93A} ALS mouse model. *Neuroscience* **164**, 975–985.

Hirokawa, N., Sobue, K., Kanda, K., Harada, A., & Yorifuji, H. (1989). The cytoskeletal architecture of the presynaptic terminal and molecular structure of synapsin 1. *J. Cell Biol.* **108**, 111–126.

Hocquemiller, M., Giersch, L., Audrain, M., Parker, S., & Cartier, N. (2016). Adeno-Associated Virus-Based Gene Therapy for CNS Diseases. *Hum. Gene Ther.* **27**, 478–496.

Inoue, A., Setoguchi, K., Matsubara, Y., Okada, K., Sato, N., Iwakura, Y., Higuchi, O., & Yamanashi, Y. (2009). Dok-7 activates the muscle receptor kinase MuSK and shapes synapse formation. *Sci. Signal.* **2**, ra7.

Ittner, L.M., Halliday, G.M., Kril, J.J., Götz, J., Hodges, J.R., & Kiernan, M.C. (2015). FTD and ALS—translating mouse studies into clinical trials. *Nat. Rev. Neurol.* **11**, 360–366.

Jablonski, M.R., Markandaiah, S.S., Jacob, D., Meng, N.J., Li, K., Gennaro, V., Lepore, A.C., Trotti, D., & Pasinelli, P. (2014). Inhibiting drug efflux transporters improves efficacy of ALS therapeutics. *Ann. Clin. Transl. Neurol.* **1**, 996–1005.

Jaiswal, M.K. (2014). Selective vulnerability of motoneuron and perturbed mitochondrial calcium homeostasis in amyotrophic lateral sclerosis: implications for motoneurons specific calcium dysregulation. *Mol. Cell. Ther.* **2**, 26.

Jiang, M., Schuster, J.E., Fu, R., Siddique, T., & Heckman, C.J. (2009). Progressive Changes in Synaptic Inputs to Motoneurons in Adult Sacral Spinal Cord of a Mouse Model of Amyotrophic Lateral Sclerosis. *J Neurosci* **29**, 15031–15038.

Johnson, J.O., Mandrioli, J., Benatar, M., et al. (2010). Exome sequencing reveals *VCP* mutations as a cause of familial ALS. *Neuron* **68**, 857–864.

Jokic, N., Gonzalez de Aguilar, J.-L., Dimou, L., Lin, S., Fergani, A., Ruegg, M. a, Schwab, M.E., Dupuis, L., & Loeffler, J.-P. (2006). The neurite outgrowth inhibitor Nogo-A promotes denervation in an amyotrophic lateral sclerosis model. *EMBO Rep.* **7**, 1162–1167.

Kanning, K.C., Kaplan, A., & Henderson, C.E. (2010). Motor neuron diversity in

development and disease. *Annu. Rev. Neurosci.* **33**, 409–440.

Katwal, a B., Konkalmatt, P.R., Piras, B. a, Hazarika, S., Li, S.S., John Lye, R., Sanders, J.M., Ferrante, E. a, Yan, Z., Annex, B.H., & French, B. A (2013). Adeno-associated virus serotype 9 efficiently targets ischemic skeletal muscle following systemic delivery. *Gene Ther.* **20**, 930–938.

Kenna, K.P., van Doormaal, P.T.C., Dekker, A.M., et al. (2016). *NEK1* variants confer susceptibility to amyotrophic lateral sclerosis. *Nat. Genet.* **48**, 1037–1042.

Kiernan, M.C., Vucic, S., Cheah, B.C., Turner, M.R., Eisen, A., Hardiman, O., Burrell, J.R., & Zoing, M.C. (2011). Amyotrophic lateral sclerosis. *Lancet* **377**, 942–955.

Kim, N., & Burden, S.J. (2008). MuSK controls where motor axons grow and form synapses. *Nat. Neurosci.* **11**, 19–27.

Kondo, T., Funayama, M., Tsukita, K., Hotta, A., Yasuda, A., Nori, S., Kaneko, S., Nakamura, M., Takahashi, R., Okano, H., Yamanaka, S., & Inoue, H. (2014). Focal Transplantation of Human iPSC-Derived Glial-Rich Neural Progenitors Improves Lifespan of ALS Mice. *Stem Cell Reports* **3**, 242–249.

Kuo, J.J., Schonewille, M., Siddique, T., Schults, A.N.A., Fu, R., Bär, P.R., Anelli, R., Heckman, C.J., & Kroese, A.B.A. (2004). Hyperexcitability of cultured spinal motoneurons from presymptomatic ALS mice. *J. Neurophysiol.* **91**, 571–575.

Kwak, S., & Kawahara, Y. (2005). Deficient RNA editing of GluR2 and neuronal death

in amyotropic lateral sclerosis. *J. Mol. Med.* **83**, 110–120.

Kwiatkowski, T.J., Bosco, D.A., Leclerc, A.L., et al. (2009). Mutations in the *FUS/TLS* gene on chromosome 16 cause familial amyotrophic lateral sclerosis. *Science* **323**, 1205–1208.

Le, N.T.T., Chang, L., Kovlyagina, I., et al. (2016). Motor neuron disease, TDP-43 pathology, and memory deficits in mice expressing ALS–FTD-linked *UBQLN2* mutations. *Proc. Natl. Acad. Sci.* **113**, E7580–E7589.

Lin, J., Zhi, Y., Mays, L., & Wilson, J.M. (2007). Vaccines based on novel adeno-associated virus vectors elicit aberrant $CD8^+$ T-cell responses in mice. *J. Virol.* **81**, 11840–11849.

Liu, Y., Pattamatta, A., Zu, T., Borchelt, D.R., Yachnis, A.T., & Ranum, L.P.W. (2016). *C9orf72* BAC Mouse Model with Motor Deficits and Neurodegenerative Features of ALS/FTD. *Neuron* **90**, 521–534.

Lucette, L., Bensimon, G., Leigh, P.N., Guillet, P., & Meininger, V. (1996). Dose-ranging study of riluzole in amyotrophic lateral sclerosis. Amyotrophic Lateral Sclerosis/Riluzole Study Group II. *Lancet* **347**, 1425–1431.

Ludolph, A.C., Bendotti, C., Blaugrund, E., et al. (2010). Guidelines for preclinical animal research in ALS/MND: A consensus meeting. *Amyotroph. Lateral Scler.* **11**, 38–45.

Maruyama, H., Morino, H., Ito, H., et al. (2010). Mutations of optineurin in amyotrophic lateral sclerosis. *Nature* **465**, 223–226.

Matsushita, T., Okada, T., Inaba, T., Mizukami, H., Ozawa, K., & Colosi, P. (2004). The adenovirus E1A and E1B19K genes provide a helper function for transfection-based adeno-associated virus vector production. *J. Gen. Virol.* **85**, 2209–2214.

Mazzini, L., Vescovi, A., Cantello, R., Gelati, M., & Vercelli, A. (2016). Stem cells therapy for ALS. *Expert Opin. Biol. Ther.* **16**, 187–199.

Meininger, V., Genge, A., van den Berg, L.H., et al. (2017). Safety and efficacy of ozanezumab in patients with amyotrophic lateral sclerosis: a randomised, double-blind, placebo-controlled, phase 2 trial. *Lancet Neurol.* **16**, 208–216.

Méjat, A., Decostre, V., Li, J., Renou, L., Kesari, A., Hantaï, D., Stewart, C.L., Xiao, X., Hoffman, E., Bonne, G., & Misteli, T. (2009). Lamin A/C-mediated neuromuscular junction defects in Emery-Dreifuss muscular dystrophy. *J. Cell Biol.* **184**, 31–44.

Meldrum, B.S. (2000). Glutamate as a neurotransmitter in the brain: review of physiology and pathology. *J. Nutr.* **130**, 1007S–1015S.

Mietzsch, M., Grasse, S., Zurawski, C., Weger, S., Bennett, A., Agbandje-McKenna, M., Muzyczka, N., Zolotukhin, S., & Heilbronn, R. (2014). OneBac: platform for scalable and high-titer production of adeno-associated virus serotype 1-12 vectors for gene therapy. *Hum. Gene Ther.* **25**, 212–222.

Murray, L.M., Talbot, K., & Gillingwater, T.H. (2010). Review: Neuromuscular synaptic vulnerability in motor neurone disease: Amyotrophic lateral sclerosis and spinal muscular atrophy. *Neuropathol. Appl. Neurobiol.* **36**, 133–156.

Okada, K., Inoue, A., Okada, M., Murata, Y., Kakuta, S., Jigami, T., Kubo, S., Shiraishi, H., Eguchi, K., Motomura, M., Akiyama, T., Iwakura, Y., Higuchi, O., & Yamanashi, Y. (2006). The muscle protein Dok-7 is essential for neuromuscular synaptogenesis. *Science* **312**, 1802–1805.

Paez-Colasante, X., Figueroa-Romero, C., Sakowski, S.A., Goutman, S.A., & Feldman, E.L. (2015). Amyotrophic lateral sclerosis: mechanisms and therapeutics in the epigenomic era. *Nat. Rev. Neurol.* **11**, 266–279.

Palace, J., Lashley, D., Newsom-Davis, J., Cossins, J., Maxwell, S., Kennett, R., Jayawant, S., Yamanashi, Y., & Beeson, D. (2007). Clinical features of the *DOK7* neuromuscular junction synaptopathy. *Brain* **130**, 1507–1515.

Parone, P.A., Da Cruz, S., Han, J.S., McAlonis-Downes, M., Vetto, A.P., Lee, S.K., Tseng, E., & Cleveland, D.W. (2013). Enhancing Mitochondrial Calcium Buffering Capacity Reduces Aggregation of Misfolded SOD1 and Motor Neuron Cell Death without Extending Survival in Mouse Models of Inherited Amyotrophic Lateral Sclerosis. *J. Neurosci.* **33**, 4657–4671.

Pérez-García, M.J., & Burden, S.J. (2012). Increasing MuSK activity delays

denervation and improves motor function in ALS mice. *Cell Rep.* **2**, 497–502.

Pieri, M., Carunchio, I., Curcio, L., Mercuri, N.B., & Zona, C. (2009). Increased persistent sodium current determines cortical hyperexcitability in a genetic model of amyotrophic lateral sclerosis. *Exp. Neurol.* **215**, 368–379.

Pollari, E., Goldsteins, G., Bart, G., Koistinaho, J., & Giniatullin, R. (2014). The role of oxidative stress in degeneration of the neuromuscular junction in amyotrophic lateral sclerosis. *Front. Cell. Neurosci.* **8**, 131.

Ravits, J., Paul, P., & Jorg, C. (2007). Focality of upper and lower motor neuron degeneration at the clinical onset of ALS. *Neurology* **68**, 1571–1575.

Renton, A.E., Majounie, E., Waite, A., et al. (2011). A hexanucleotide repeat expansion in *C9ORF72* is the cause of chromosome 9p21-linked ALS-FTD. *Neuron* **72**, 257–268.

Rosen, D.R., Siddique, T., Patterson, D., Figlewicz, D.A., Sapp, P., Hentati, A., Donaldson, D., Goto, J., O'Regan, J.P., & Deng, H.X. (1993). Mutations in Cu/Zn superoxide dismutase gene are associated with familial amyotrophic lateral sclerosis. *Nature* **362**, 59–62.

Sanes, J.R., & Lichtman, J.W. (1999). Development of the vertebrate neuromuscular junction. *Annu. Rev. Neurosci.* **22**, 389–442.

Scott, S., Kranz, J.E., Cole, J., Lincecum, J.M., Thompson, K., Kelly, N., Bostrom, A., Theodoss, J., Al-Nakhala, B.M., Vieira, F.G., Ramasubbu, J., & Heywood, J.A. (2008).

Design, power, and interpretation of studies in the standard murine model of ALS. *Amyotroph. Lateral Scler.* **9**, 4–15.

Sharma, A., Lyashchenko, A.K., Lu, L., Nasrabady, S.E., Elmaleh, M., Mendelsohn, M., Nemes, A., Tapia, J.C., Mentis, G.Z., & Shneider, N.A. (2016). ALS-associated mutant FUS induces selective motor neuron degeneration through toxic gain of function. *Nat. Commun.* **7**, 10465.

Silverman, J.M., Fernando, S.M., Grad, L.I., Hill, A.F., Turner, B.J., Yerbury, J.J., & Cashman, N.R. (2016). Disease Mechanisms in ALS: Misfolded SOD1 Transferred Through Exosome-Dependent and Exosome-Independent Pathways. *Cell. Mol. Neurobiol.* **36**, 377–381.

Sleigh, J.N., Grice, S.J., Burgess, R.W., Talbot, K., & Cader, M.Z. (2014). Neuromuscular junction maturation defects precede impaired lower motor neuron connectivity in Charcot-Marie-Tooth Type 2D mice. *Hum. Mol. Genet.* **23**, 2639–2650.

Spalloni, A., Nutini, M., & Longone, P. (2013). Role of the N-methyl-d-aspartate receptors complex in amyotrophic lateral sclerosis. *Biochim. Biophys. Acta - Mol. Basis Dis.* **1832**, 312–322.

Sreedharan, J., Blair, I.P., Tripathi, V.B., et al. (2008). TDP-43 mutations in familial and sporadic amyotrophic lateral sclerosis. *Science* **319**, 1668–1672.

Taetzsch, T., Tenga, M.J., & Valdez, G. (2017). Muscle fibers secrete FGFBP1 to slow

degeneration of neuromuscular synapses during aging and progression of ALS. *J. Neurosci.* **37**, 70–82.

Takahashi, Y., Fukuda, Y., Yoshimura, J., et al. (2013). Erbb4 mutations that disrupt the neuregulin-erbb4 pathway cause amyotrophic lateral sclerosis type 19. *Am. J. Hum. Genet.* **93**, 900–905.

Takuma, H., Kwak, S., Yoshizawa, T., & Kanazawa, I. (1999). Reduction of GluR2 RNA editing, a molecular change that increases calcium influx through AMPA receptors, selective in the spinal ventral gray of patients with amyotrophic lateral sclerosis. *Ann. Neurol.* **46**, 806–815.

Tassi, E., Walter, S., Aigner, A., Cabal-Manzano, R.H., Ray, R., Reier, P.J., & Wellstein, A. (2007). Effects on neurite outgrowth and cell survival of a secreted fibroblast growth factor binding protein upregulated during spinal cord injury. *Am. J. Physiol. Regul. Integr. Comp. Physiol.* **293**, R775–R783.

Taylor, J.P., Brown, R.H., & Cleveland, D.W. (2016). Decoding ALS: from genes to mechanism. *Nature* **539**, 197–206.

Tomono, T., Hirai, Y., Okada, H., Adachi, K., Ishii, A., Shimada, T., Onodera, M., Tamaoka, A., & Okada, T. (2016). Ultracentrifugation-free chromatography-mediated large-scale purification of recombinant adeno-associated virus serotype 1 (rAAV1). *Mol. Ther. Methods Clin. Dev.* **3**, 15058.

Valdez, G., Tapia, J.C., Lichtman, J.W., Fox, M.A., & Sanes, J.R. (2012). Shared resistance to aging and als in neuromuscular junctions of specific muscles. *PLoS One* **7**, e34640.

Vance, C., Rogelj, B., Hortobagyi, T., et al. (2009). Mutations in FUS, an RNA processing protein, cause familial amyotrophic lateral sclerosis type 6. *Science* **323**, 1208–1211.

Wu, D., Kan, M., Sato, G.H., Okamoto, T., & Denry Sato, J. (1991). Characterization and molecular cloning of a putative binding protein for heparin-binding growth factors. *J. Biol. Chem.* **266**, 16778–16785.

Yamashita, T., Chai, H.L., Teramoto, S., Tsuji, S., Shimazaki, K., Muramatsu, S. ichi, & Kwak, S. (2013). Rescue of amyotrophic lateral sclerosis phenotype in a mouse model by intravenous AAV9-ADAR2 delivery to motor neurons. *EMBO Mol. Med.* **5**, 1710–1719.

Yoo, Y.E., & Ko, C.P. (2012). Dihydrotestosterone ameliorates degeneration in muscle, axons and motoneurons and improves motor function in amyotrophic lateral sclerosis model mice. *PLoS One* **7**, e37258.

Yumoto, N., Kim, N., & Burden, S.J. (2012). Lrp4 is a retrograde signal for presynaptic differentiation at neuromuscular synapses. *Nature* **489**, 438–442.

Zahavi, E.E., Ionescu, A., Gluska, S., Gradus, T., Ben-Yaakov, K., & Perlson, E.

(2015). A compartmentalized microfluidic neuromuscular co-culture system reveals spatial aspects of GDNF functions. *J. Cell Sci.* **128**, 1241–1252.

Zhang, B., Luo, S., Wang, Q., Suzuki, T., Xiong, W.C., & Mei, L. (2008). LRP4 Serves as a Coreceptor of Agrin. *Neuron* **60**, 285–297.

Zhu, S., Stavrovskaya, I.G., Drozda, M., et al. (2002). Minocycline inhibits cytochrome c release and delays progression of amyotrophic lateral sclerosis in mice. *Nature* **417**, 74–78.

Zhu, Y., Fotinos, A., Mao, L.L.J., Atassi, N., Zhou, E.W., Ahmad, S., Guan, Y., Berry, J.D., Cudkowicz, M.E., & Wang, X. (2015). Neuroprotective agents target molecular mechanisms of disease in ALS. *Drug Discov. Today* **20**, 65–75.

Zincarelli, C., Soltys, S., Rengo, G., & Rabinowitz, J.E. (2008). Analysis of AAV serotypes 1-9 mediated gene expression and tropism in mice after systemic injection. *Mol. Ther.* **16**, 1073–1080.

6. Figures 1–13 and figure legends

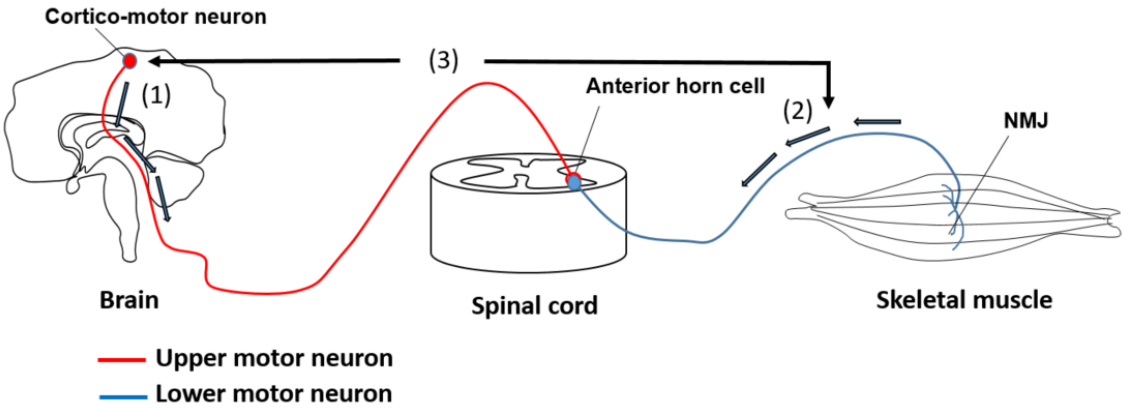

Figure 1. Schematic diagram of disease progression models of neurodegeneration in ALS.

Three disease progression models of neurodegeneration in ALS. (1) The "dying-forward" hypothesis proposes that ALS is mainly a disorder of cortico-motoneurons, which connect monosynaptically to anterior horn cells, thereby mediating the anterograde degeneration of anterior horn cells via glutamate-mediated excitotoxicity. (2) The "dying-back" hypothesis proposes that motor neuron degeneration first becomes evident as a size-reduction of the motor nerve terminals and subsequent denervation at NMJs. Motor neuron degeneration then progresses proximally. (3) The independent neurodegeneration" hypothesis proposes that upper and lower motor neurons degenerate independently at the same time.

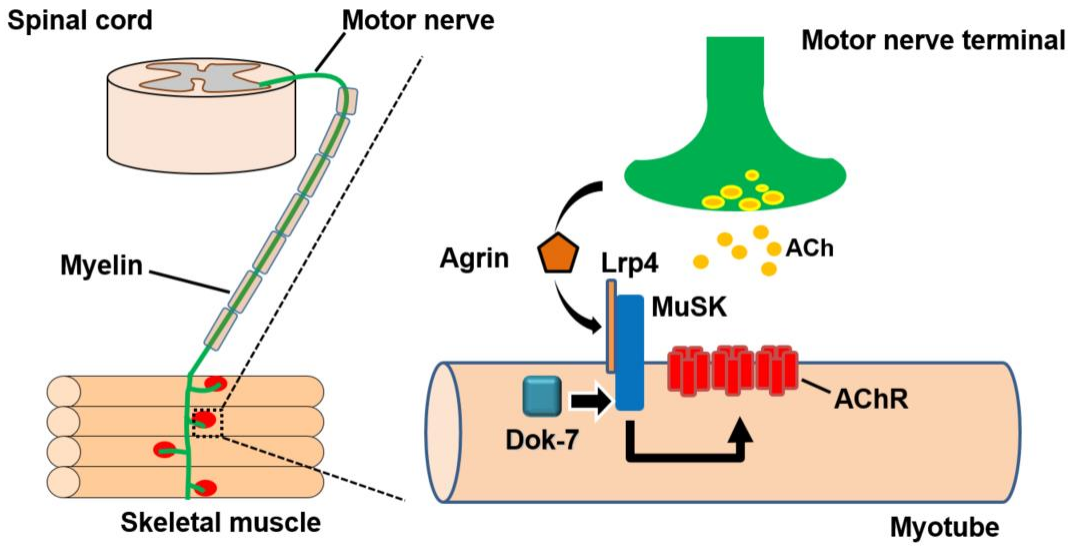

Figure 2. Schematic diagram of the neuromuscular junction (NMJ) and signaling involved in NMJ formation.

NMJ is a synapse formed between myelinated motor nerves and skeletal muscle. In transmission at mammalian NMJs, acetylcholine (ACh) is released from the motor nerve terminal into the synaptic cleft and binds to AChRs in the postsynaptic muscle membrane to open their ion channels. The formation and maintenance of NMJs are orchestrated by the muscle-specific receptor tyrosine kinase MuSK. Activation of MuSK requires the motor neuron-secreted activator agrin, which activates MuSK via binding to the MuSK co-receptor Lrp4, and Dok-7, an essential muscle-intrinsic MuSK activator.

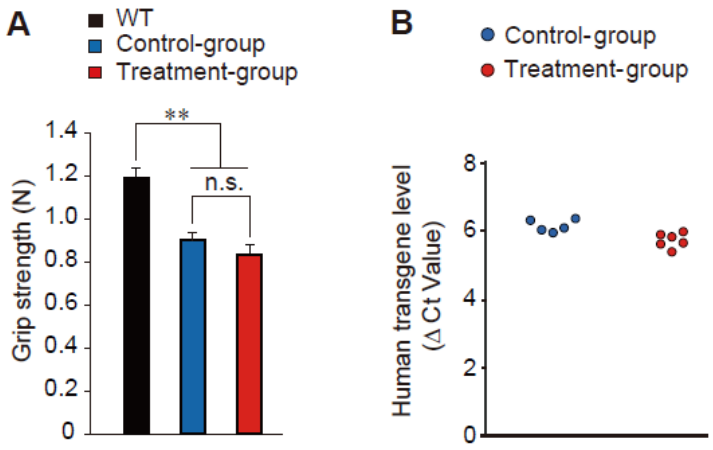

Figure 3. Grip strength was similarly impaired before treatment and h*SOD1* transgene copy number was comparable in the treatment- and control-groups of ALS mice.

(**A**) Forelimb grip strength of wild-type (WT) mice and that of control- and AAV-D7 treatment-groups of ALS mice at P84 (*n* = 5 or 6 mice). Values are means ± s.e.m. ***P* = 0.0016 (WT vs control-group) and 0.0003 (WT vs treatment-group) by one-way analysis of variance (ANOVA) with Bonferroni's test. n.s., not significant. (**B**) The difference in cycle threshold (ΔCt) between the human *SOD1-G93A* transgene and the reference mouse *apob* gene.

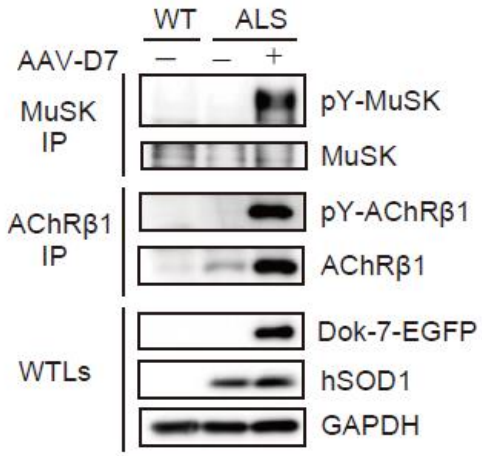

Figure 4. *DOK7* gene therapy enhances phosphorylation of MuSK and AChR β1 subunit in ALS mice.

Wild-type (WT) or ALS mice treated or not with 1.2×10^{12} vg of AAV-D7 at P90 were subjected to the following assay at P120. Tyrosine phosphorylation of MuSK or AChR in the hind-limb muscle. MuSK or AChRβ1-subunit (AChRβ1) immunoprecipitates (IP) from whole tissue lysates (WTLs) of the hind-limb muscle were immunoblotted for phosphotyrosine (pY), MuSK and AChRβ1. WTLs were blotted for Dok-7-EGFP, human SOD1, and GAPDH.

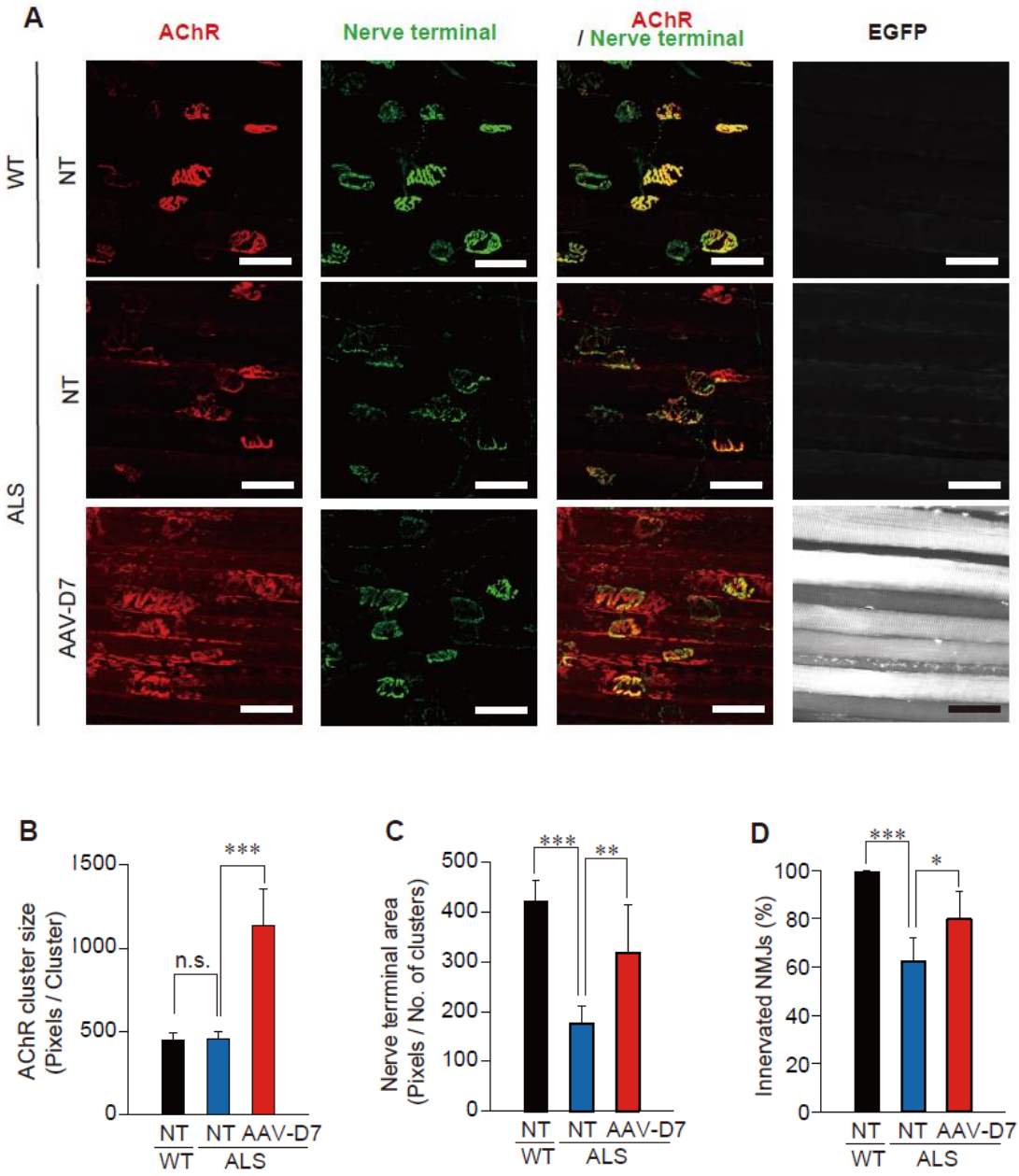

Figure 5. *DOK7* gene therapy suppresses motor nerve terminal degeneration at the NMJ in ALS mice.

Wild-type (WT) or ALS mice treated or not with 1.2×10^{12} vg of AAV-D7 at P90 were subjected to the following assays at P120. (**A**) Whole-mount staining of NMJs on the diaphragm muscle. Motor nerve terminals (green) and postsynaptic AChRs (red) were

stained with anti-synapsin-1 antibodies and α-bungarotoxin, respectively. Expression of Dok-7-EGFP fusion protein (gray) was monitored by EGFP. The size of each motor nerve terminal (**B**), AChR cluster (**C**) and innervation ratio (**D**) were quantified (WT-NT, $n = 5$ mice; ALS-NT, $n = 5$ mice; ALS-AAV-D7, $n = 6$ mice). Values are means ± s.d. (B) ***$P < 0.0001$; (C) **$P = 0.0077$, ***$P = 0.0001$; (D) *$P = 0.0134$, ***$P < 0.0001$ by one-way ANOVA with Dunnett's test. Scale bars, 50 μm. NT, not treated. n.s., not significant.

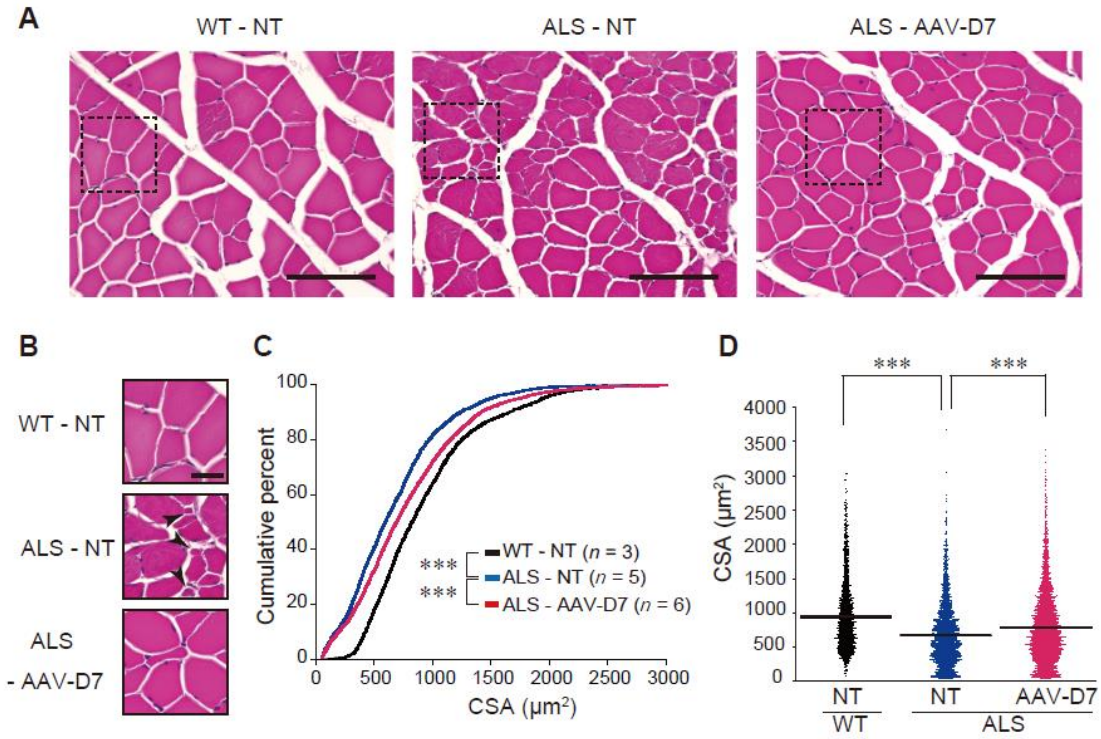

Figure 6. *DOK7* gene therapy suppresses myofiber atrophy in ALS mice.

WT or ALS mice treated or not with 1.2×10^{12} vg of AAV-D7 at P90 were analyzed at P120. (**A**) H&E staining of transverse sections of tibialis anterior muscle. Scale bars, 100 μm. NT, not treated. (**B**) Magnifications of respective boxes in A. Arrowheads indicate severe myofiber atrophy in ALS-NT. Scale bars, 25 μm. (**C**) Cumulative percentage of myofiber cross-section area (CSA). (**D**) Individual and mean CSA (WT-NT, *n* = 3 mice; ALS-NT, *n* = 5 mice; ALS-AAV-D7, *n* = 6 mice). ***$P < 0.0001$ by Kolmogorov–Smirnov test (b) and by one-way ANOVA with Dunnett's test (c).

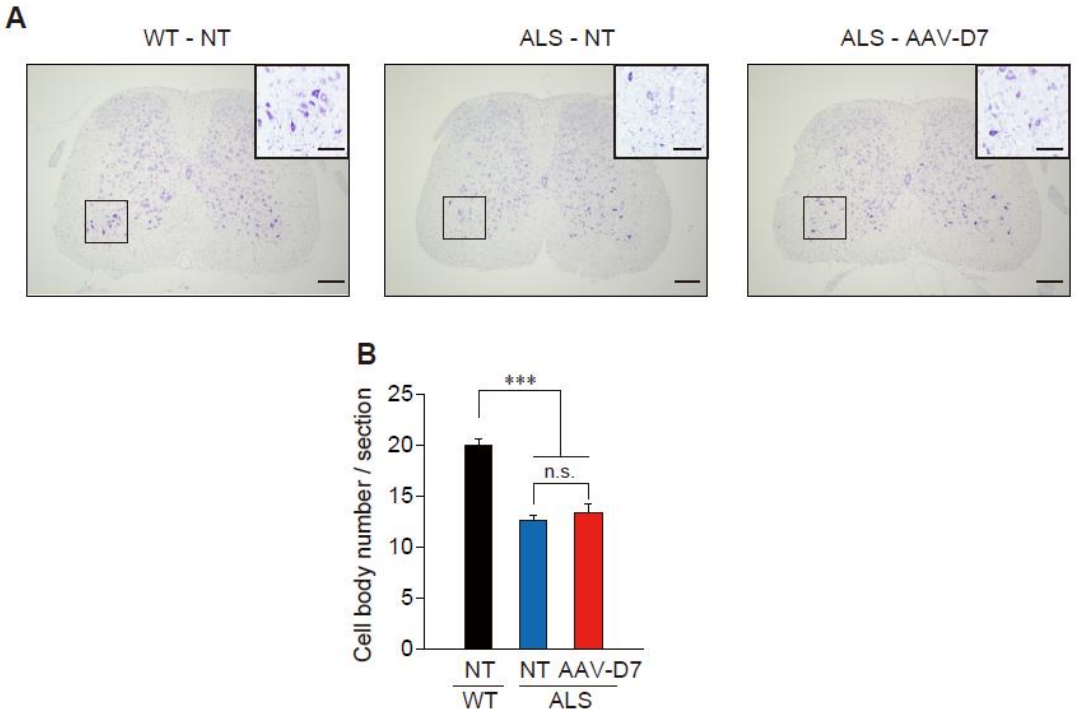

Figure 7. *DOK7* gene therapy shows no obvious effects on motor neuron survival in ALS mice.

WT or ALS mice treated or not with 1.2×10^{12} vg of AAV-D7 at P90 were analyzed at P120. (**A**) Nissl staining of the L4-L5 spinal segment. Scale bars, 200 μm. Insets show higher magnification of the ventral horn in the boxed regions (Scale bars, 50 μm). (**B**) Quantification of surviving motor neurons ($n = 5$ mice). Values are means ± s.e.m. ***$P < 0.0001$ by one-way ANOVA with Bonferroni's test. NT, not treated. n.s., not significant.

.

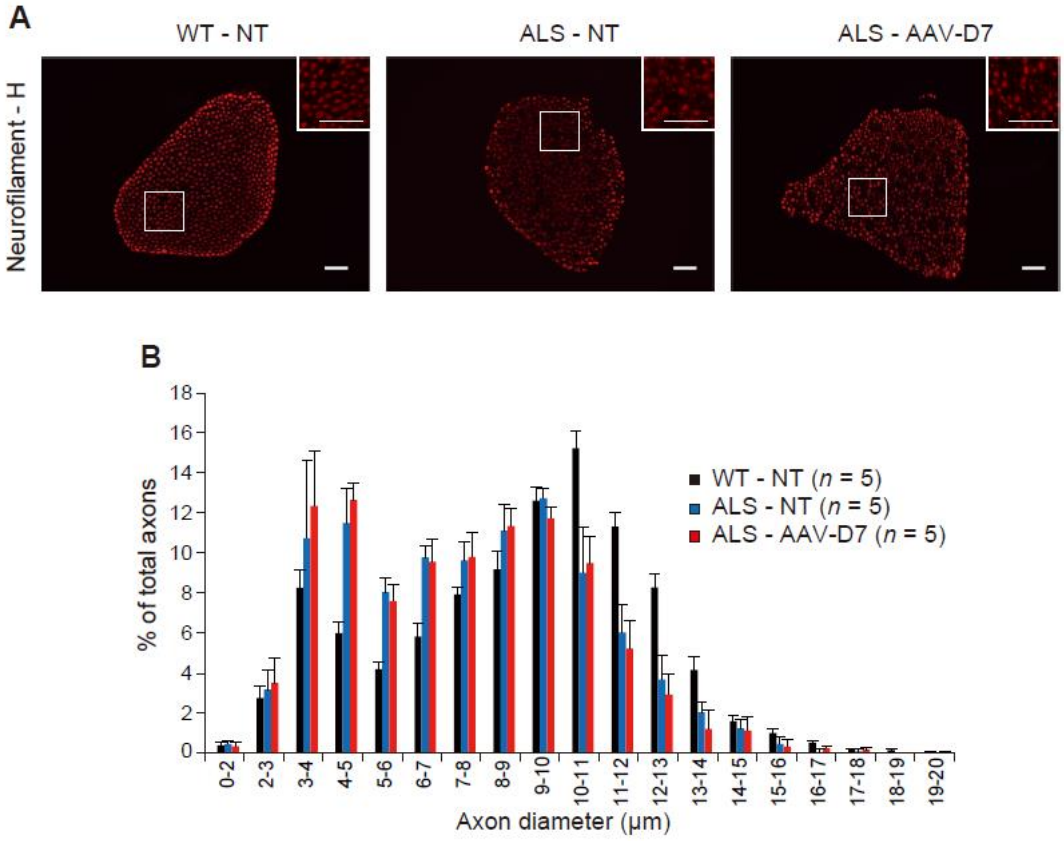

Figure 8. *DOK7* gene therapy shows no obvious effects on motor axon atrophy in ALS mice.

WT or ALS mice treated or not with 1.2×10^{12} vg of AAV-D7 at P90 were analyzed at P120. (**A**) Anti-neurofilament-H staining of the L4 ventral roots. Insets show higher magnification of the boxed regions. Scale bars, 50 µm. NT, not treated. (**B**) Size distribution of motor axons (n = 5 mice). Values are means ± s.e.m.

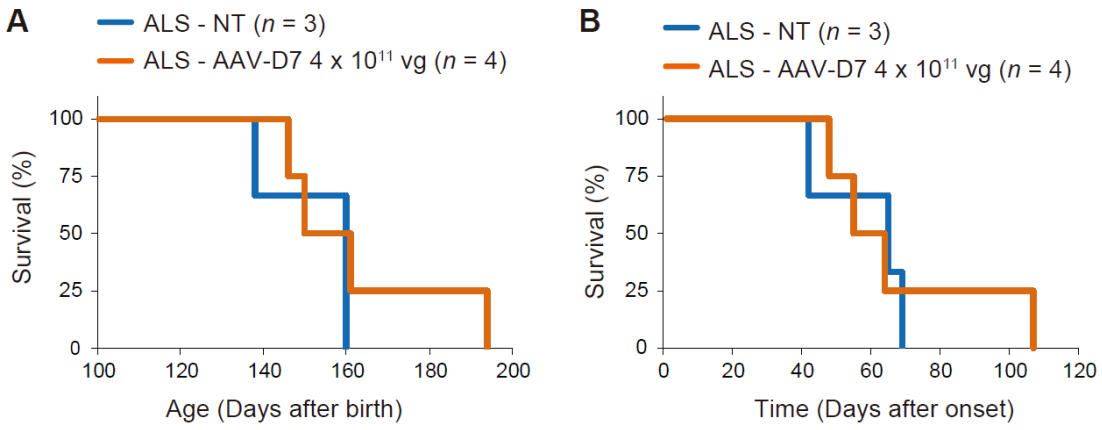

Figure 9. A dosage of 4 × 10^{11} vg of AAV-D7 was not a sufficient treatment for ALS mice in the preliminary experiment.

ALS mice were treated or not with 4 × 10^{11} vg of AAV-D7 at individually defined disease onset (ALS-NT, *n* = 3 mice; ALS-AAV-D7, *n* = 4 mice). (**A**) Kaplan–Meier survival curves after birth of untreated ALS mice and AAV-D7-treated ALS mice. NT, not treated. (**B**) Kaplan–Meier survival curves after onset of untreated ALS mice and AAV-D7-treated ALS mice.

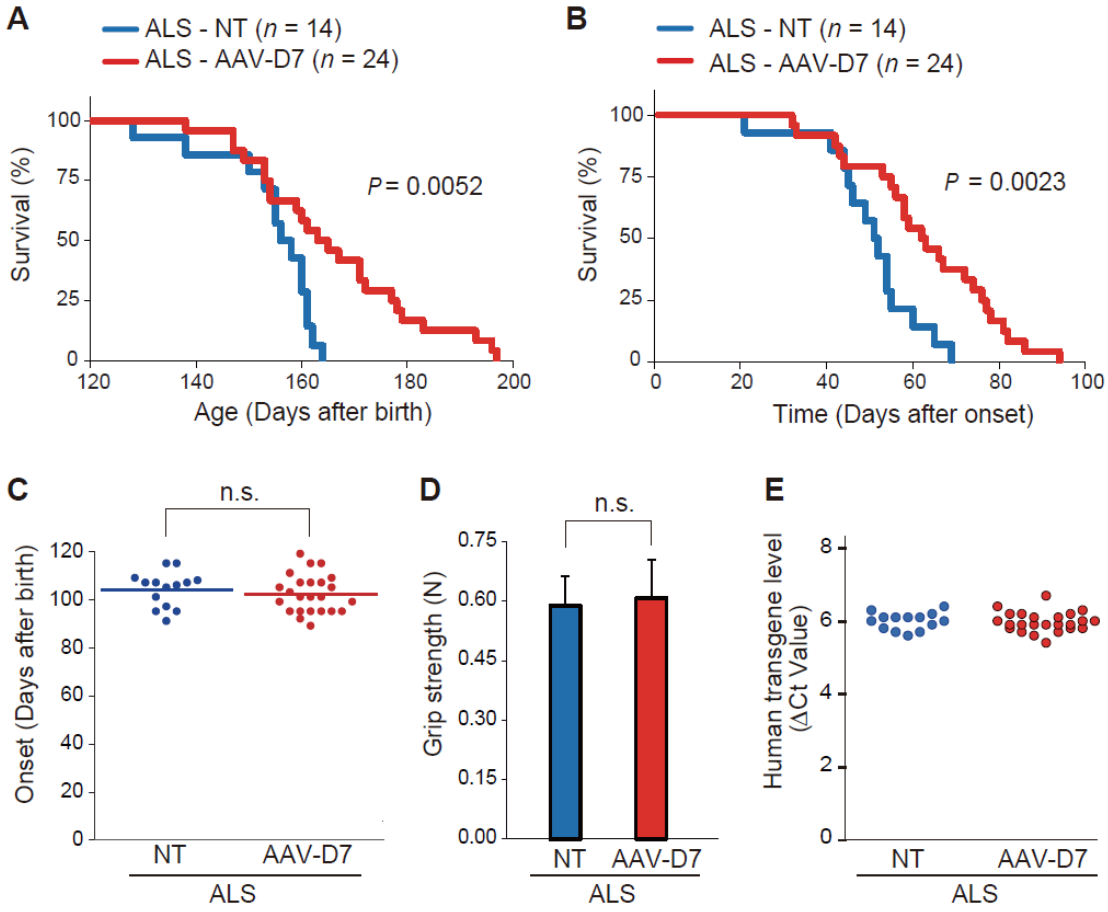

Figure 10. *DOK7* gene therapy prolongs life span in ALS mice.

ALS mice were treated or not with 1.2 × 10^{12} vg of AAV-D7 at individually defined disease onset (ALS-NT, *n* = 14 mice; ALS-AAV-D7, *n* = 24 mice). (**A**) Kaplan–Meier survival curves after birth of untreated ALS mice (154.4 ± 2.7 days, mean ± s.e.m.) and AAV-D7-treated ALS mice (166.3 ± 3.2 days). *P* = 0.0052 by log-rank test. NT, not treated. (**B**) Kaplan–Meier survival curves after onset of untreated ALS mice (50.3 ± 3.1 days, mean ± s.e.m.) and AAV-D7-treated ALS mice (64.2 ± 3.3 days). *P* = 0.0023 by log-rank test. (**C**) Ages at onset for untreated and AAV-D7-treated ALS mice. Mean ages

of onset were indicated by horizontal bars. (**D**) Forelimb grip strength of ALS mice at onset in untreated and AAV-D7-treated groups. Values are means ± s.e.m. n.s., not significant by Student's t-test (C, D). (**E**) The difference in cycle threshold (ΔCt) between the human SOD1-G93A transgene and the reference mouse *apob* gene.

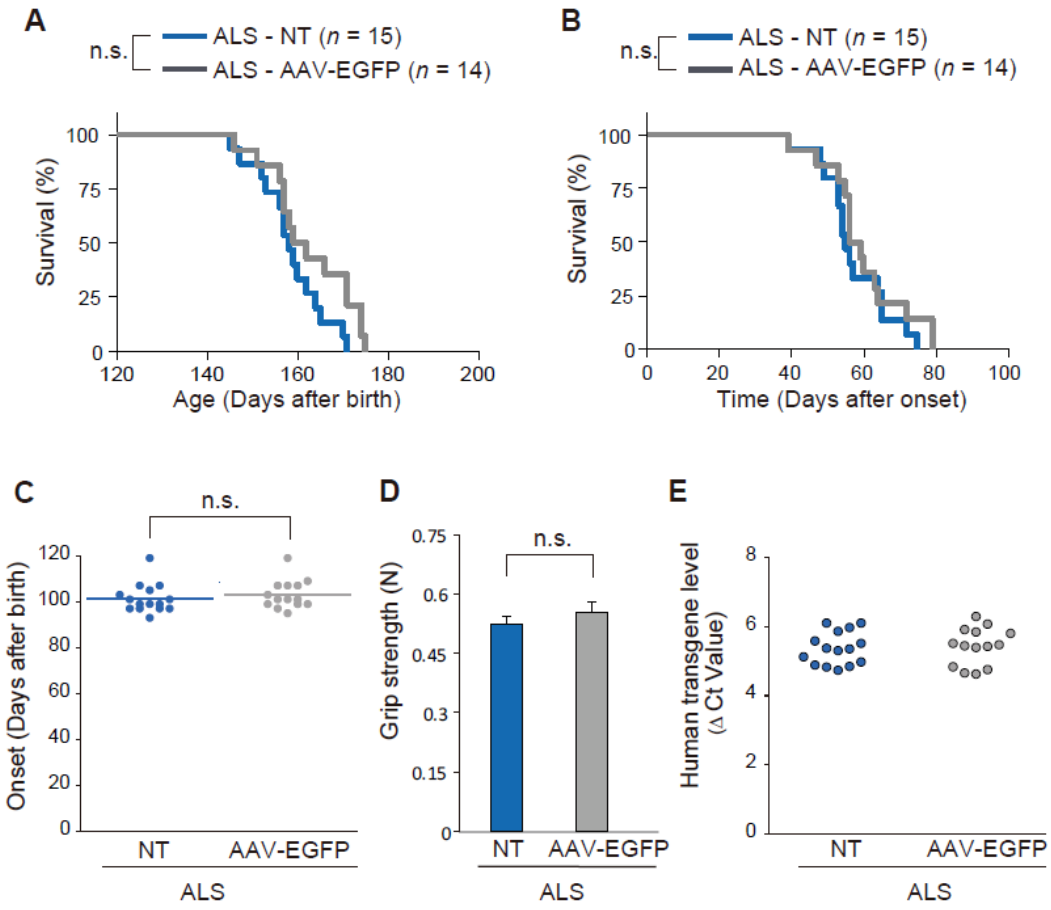

Figure 11. Treatment with AAV-EGFP does not prolong survival in ALS mice.

ALS mice were treated or not with 1.2×10^{12} vg of AAV-EGFP at individually defined disease onset (ALS-NT, *n* = 15 mice; ALS-AAV-EGFP, *n* = 14 mice). Kaplan–Meier survival curves after birth of untreated ALS mice (158.4 ± 1.9 days, mean ± s.e.m.) and AAV-EGFP-treated ALS mice (162.1 ± 2.5 days). n.s., not significant by log-rank test. NT, not treated. (**B**) Kaplan–Meier survival curves after onset of untreated ALS mice (57.3 ± 2.4 days, mean ± s.e.m.) and AAV-EGFP-treated ALS mice (59.8 ± 3.0 days). n.s., not significant by log-rank test. (**C**) Ages of onset for untreated and AAV-EGFP-

treated ALS mice. Mean ages of onset were indicated by horizontal bars. (**D**) Forelimb grip strength of ALS mice at onset in untreated and AAV-EGFP-treated groups. Values are means ± s.e.m. n.s., not significant by Student's t-test (C, D). (**E**) The difference in cycle threshold (ΔCt) between the human SOD1-G93A transgene and the reference mouse *apob* gene.

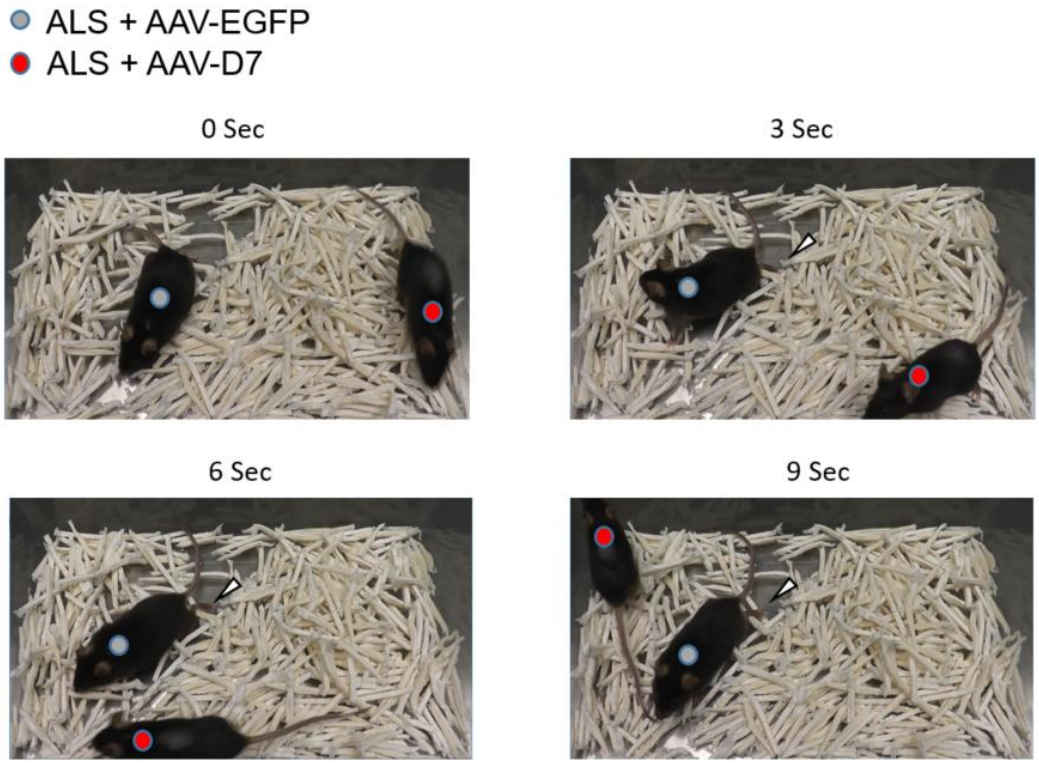

Figure 12. *DOK7* gene therapy apparently improved motor activity of an ALS mouse at P150.

The AAV-EGFP-treated mouse (marked by a gray circle) was dragging its hind limbs (arrow heads), indicative of paralysis, and had impaired mobility. By contrast, the AAV-D7-treated mouse (marked by a red circle) showed improved mobility sufficient to explore the cage. Individually defined disease onset was the same (P115) for both mice as indicated.

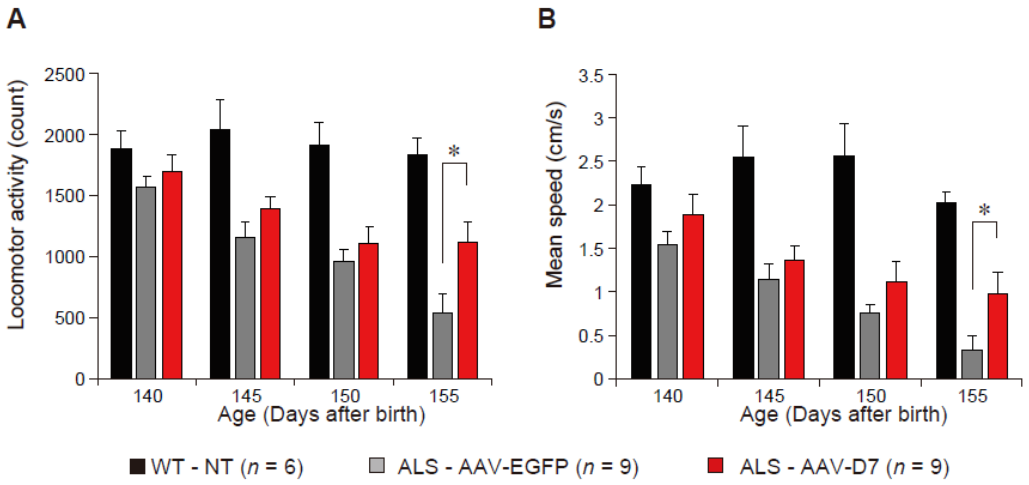

Figure 13. *DOK7* gene therapy improves motor activity in ALS mice.

WT or ALS mice treated with 1.2×10^{12} vg of AAV-EGFP or AAV-D7 at the individually defined disease onset were subjected to the open field tests at the indicated ages (WT-NT, n = 6 mice; ALS-AAV-EGFP, n = 9 mice; ALS-AAV-D7, n = 9 mice). Spontaneous motor activity was represented by the locomotor activity (**A**) and mean speed (**B**). Values are means ± s.e.m. (A) *P = 0.0244, (B) *P = 0.0349 by Mann–Whitney U-test. NT, not treated

7. Acknowledgments

I would like to express my sincere gratitude to the people who helped me to complete this thesis. First, I would like to express my deepest gratitude to my supervisor Dr. Yuji Yamanashi for insightful comments, warm encouragement and providing a blessed environment.

I would like to express great appreciation for my dissertation committee. I thank Dr. Yuichi Iino for his guidance and support. I thank Dr. Atsu Aiba, Dr. Mutsuhiro Takekawa, and Dr. Makoto Nakanishi for their valuable suggestions and great encouragement throughout this process.

I thank Dr. Takashi Okada and Mr. Taro Tomono for their collaboration in producing the virus vector and their thoughtful comments. I thank Dr. Hitoshi Okazawa and Dr. Chisato Yoshida for technical advice and helpful discussions regarding histological analysis of motor neurons and Dr. R. F. Whittier for critical reading of this manuscript and thoughtful discussions. I also thank Dr. James M. Wilson for providing the AAV packaging plasmid (pRep2Cap9) and Dr. Masanori Nojima for advice on statistical analyses.

I would like to express my cordial gratitude to all of my fellow laboratory members. This work was completed with their kind support and guidance. I am grateful to Dr. Tohru Tezuka for his warm guidance during my study. I thank Dr. Sumimasa Arimura for technical advice and thoughtful discussions. I also thank Dr. Ryo Ueta for critical reading of this manuscript and thoughtful discussions.

Finally, I thank my family.